Touch sensation requires the mechanically gated ion channel ELKIN1

Chakrabarti S., Klich J.D., Khallaf M.A., Hulme A.J., Sánchez-Carranza O., Baran Z.M., Rossi A., Huang A.T.L., Pohl T., Fleischer R., Fürst C., Hammes A., Bégay V., Hörnberg H., Finol-Urdaneta R.K., Poole K., Dottori M., Lewin G.

Science
2024 MAR 01 ; 383(6686): 992-998
2024 FEB 29 (first published online: final publication)
doi: 10.1126/science.adl0495

Publisher: American Association for the Advancement of Science (AAAS)

Touch sensation requires the mechanically-gated ion channel ELKIN1.

Authors

Sampurna Chakrabarti[1], Jasmin D. Klich[1], Mohammed A. Khallaf[1,2], Amy J. Hulme[3], Oscar Sánchez-Carranza[1], Zuzanna M. Baran[1,4], Alice Rossi[1], Angela Tzu-Lun Huang[1], Tobias Pohl[4], Raluca Fleischer[1], Carina Fürst[1,5], Annette Hammes[5], Valérie Bégay[1], Hanna Hörnberg[4,6], Rocio K. Finol-Urdaneta[3], Kate Poole[7], Mirella Dottori[3], Gary R. Lewin[1,8,9*]

Affiliations:

[1]Molecular Physiology of Somatic Sensation Laboratory, Max Delbrück Center for Molecular Medicine in the Helmholtz Association (MDC), Robert Rössle Str. 10, 13125 Berlin-Buch, Germany.

[2]Department of Zoology and Entomology, Faculty of Science, Assiut University, Assiut, 71516 Egypt

[3]School of Medical, Indigenous and Health Sciences, Molecular Horizons, University of Wollongong, Wollongong, NSW, 2522, Australia

[4]Molecular and Cellular Basis of Behavior, Max Delbrück Center for Molecular Medicine in the Helmholtz Association (MDC), Robert Rössle Str. 10, 13125 Berlin-Buch, Germany.

[5]Molecular Pathways in Cortical Development, Max Delbrück Center for Molecular Medicine in the Helmholtz Association (MDC), Robert Rössle Str. 10, 13125 Berlin-Buch, Germany.

[6]NeuroCure Cluster of Excellence, Humboldt-Universität zu Berlin, Unter den Linden 6, 10117 Berlin, Germany

[7]School of Biomedical Sciences, Faculty of Medicine & Health, University of New South Wales, Sydney, NSW 2052, Australia.

[8]Charité-Universitätsmedizin Berlin, Charitéplatz 1, 10117 Berlin, Germany

[9]German Center for Mental Health (DZPG), partner site Berlin.

[*]Correspondence to glewin@mdc-berlin.de

Abstract

Touch perception is enabled by mechanically-activated ion channels, the opening of which excites cutaneous sensory endings to initiate sensation. We identify ELKIN1 as an ion channel likely gated by mechanical force, necessary for normal touch sensitivity in mice. Touch insensitivity in *Elkin1*$^{-/-}$ mice was caused by a loss of mechanically-activated currents (MA-currents) in around half of all sensory neurons activated by light touch (low threshold mechanoreceptors, LTMRs). Reintroduction of *Elkin1* into sensory neurons from *Elkin1*$^{-/-}$ mice restored MA-currents. Additionally, siRNA-mediated knockdown of *ELKIN1* from induced human sensory neurons substantially reduced indentation-induced MA-currents supporting a conserved role for ELKIN1 in human touch. Our data identify ELKIN1 as a core component of touch transduction in mice and potentially in humans.

One-Sentence Summary:

ELKIN1 is an ion channel important for touch in mice and potentially humans.

Main Text:

Touch sensation is fundamental to our sense of self, social interactions and exploration of the tactile world(*1*, *2*). Sensation is initiated at specialized end-organs in the skin, innervated by low threshold mechanoreceptors (LTMRs) with their cell bodies in the dorsal root ganglion (DRG). The peripheral endings of LTMRs are equipped with mechanically-gated ion channels that can be opened by very small forces to initiate and enable touch perception(*3*, *4*). The mechanically-gated ion channel PIEZO2 is expressed by most sensory neurons in the DRG(*5*) and in its absence, around half of LTMRs no longer respond to mechanical stimuli(*6*–*8*). The DRG also contains so-called nociceptors, sensory neurons specialized to detect potentially damaging and painful stimuli, including intense mechanical force(*3*). Many nociceptors express PIEZO2 channels, but remain mechanosensitive in its absence. The preservation of mechanosensitivity in many LTMRs in the absence of PIEZO2 channels(*6*–*8*) led us to search for other mechanically-gated ion channels that could account for PIEZO2-independent sensory mechanotransduction.

ELKIN1 can detect mechanical force.

We previously identified ELKIN1 (TMEM87A) as a protein that is both necessary and sufficient to confer mechanosensitivity to highly metastatic human melanoma cells(*9*). Cryo-EM structures of human ELKIN1 recently revealed a monomeric 7 transmembrane protein with an N-terminal extracellular Golgi-dynamics domain fold (GOLD-domain)(*10*). A second higher resolution structure recently identified a cation conduction pathway through the protein(*11*). We overexpressed *Elkin1* in HEK293T cells lacking PIEZO1 channels (HEK293T$^{Piezo1-/-}$ cells)(*12*) and found large indentation-induced mechanically-activated currents (MA-currents) in a majority of transfected cells (Fig 1A,B). Cells were plated on laminin 511 and poly-L-lysine (PLL), a substrate that supports increased mechanosensitivity(*13*); untransfected cells showed no indentation-induced currents. ELKIN1-dependent currents were rapidly-adapting (RA) with fast inactivation time constants (<10 ms), similar to those of PIEZO2 ion channels(*5*, *14*) (Fig 1 A,B,C). Using substrate deflection via pillar arrays(*9*, *14*), we also found robust mechanically-activated currents in all HEK293T$^{Piezo1-/-}$ cells, transfected with *Elkin1* expression constructs, but also in cells transfected with *Elkin1* lacking the N-terminal GOLD-domain (*Elk1Δ170*) (Fig 1C,D, Fig. S1A)(*9*). Most of the pillar evoked currents were rapidly-adapting (RA,

inactivation <10 ms), or intermediately adapting (IA, inactivation between 10-50 ms). Measurements of pillar gated currents at different holding potentials revealed a linear current-voltage relation with a reversal potential of 0 mV for both *Elkin1* and *Elk1Δ170* transfected cells (Fig 1E). Therefore, our results suggest that the GOLD-domain is not necessary for mechanical activation of ELKIN1. ELKIN1 currents showed a distinctive pharmacological profile, being sensitive to the non-specific pore-blocker Gd^{3+}(30 μM), but barely affected by ruthenium red (30 μM), a compound that completely blocks other mechanosensitive channels like PIEZO1 and PIEZO2 (*5*, *15*) (Fig 1F, Fig S1B). Additionally, in agreement with recent reports (*11*, *15*) we found that cells expressing mouse *Elkin1* display prominent leak currents at very positive (> +60 mV) and very negative potentials (< -100 mV) (Fig 1G, Fig S1C). ELKIN1 reconstituted into proteoliposomes reportedly show single channel activity at very positive potentials(*16*). We also found that *Elkin1* transfected HEK293T$^{Piezo1-/-}$ cells showed currents, which were substantially potentiated by application of mild positive pressure pulses (20 mm of Hg) applied via the cell attached pipette (Fig S2A,B,C). Therefore, we provide multiple lines of evidence that ELKIN1 is likely an ion channel that can detect mechanical force.

Mouse sensory neurons express ELKIN1.

We hypothesized that ELKIN1 could also be involved in mammalian touch sensation. We generated a CRISPR/Cas9 mediated genomic deletion of the mouse *Tmem87a/Elkin1* gene locus spanning sequences coding for transmembrane domains 2-6, that includes the proposed ion conduction pathway (Fig S3A)(*11*). Mice homozygous for the genomic deletion (*Elkin1*$^{-/-}$ mice) were viable and born at the expected Mendelian ratios (WT: 25.7%, *Elkin1*$^{+/-}$: 46.2%, *Elkin1*$^{-/-}$: 28% n=132, Table S2). Single molecule fluorescent *in situ* hybridization (smFISH) and immunohistochemistry with an antibody against ELKIN1 showed that *Elkin1*$^{-/-}$ mice were complete null mutants (Fig 2A). Our validated ELKIN1 antibody revealed that ELKIN1 protein levels appeared to be especially high in sensory neurons of the DRG. ELKIN1 protein was robustly detected in all subsets of DRG neurons, consistent with single cell expression data from mice, macaques and humans(*17*–*21*); around 60% of neurons showed high ELKIN1 levels (Fig S3B,C). Sensory neurons expressing high amounts of ELKIN1 made up 34% of neurofilament

heavy chain positive (NF200$^+$) large neurons with myelinated axons. High ELKIN1 expression was also found in 75% of isolectin-B4 positive (IB4$^+$) non-peptidergic small neurons(*22*) and 45% of small neurons positive for the capsaicin-gated Transient receptor potential channel, TRPV1 (Fig S3B,C). Both of these two neurochemically distinct nociceptor types are reported to be responsive to mechanical force(*23*).

Sensory deficits in *Elkin1*$^{-/-}$ mice.

The absence of ELKIN1 did not alter the neurochemical make-up of the sensory ganglia as the percentage of DRG neurons positive for markers like NF200, IB4, TRPV1 and tyrosine hydroxylase (TH) was unchanged in the *Elkin1*$^{-/-}$ mice compared to wild types (WT) (Fig 2B). Ultrastructural analysis of the saphenous nerve revealed no pathology or loss of myelinated or unmyelinated axons in *Elkin1*$^{-/-}$ mice (Fig 2C, table S1). However, behavioral indicators of touch sensitivity, like percentage of responses to a cotton swab, were profoundly reduced in *Elkin1*$^{-/-}$ mice compared to WT animals (WT: 90% vs. *Elkin1*$^{-/-}$: 47.5% paw withdrawal, $p<0.0001$, unpaired Student's t-test, Fig 2D). Paw withdrawal thresholds to von Frey filaments were also significantly elevated ($p<0.0001$, two-way ANOVA with Sidak post hoc test), with substantial deficits observed across a range of von Frey force filaments in *Elkin1*$^{-/-}$ mice (Fig 2E). However, responses to brush stimuli in *Elkin1*$^{-/-}$ were similar to WT mice (Fig S3E). These results confirm reduced sensitivity to mechanical forces in *Elkin1*$^{-/-}$ mice. However, non-mechanosensory modalities, like heat withdrawal thresholds, were unaltered in *Elkin1*$^{-/-}$ mice (Fig S3D). *Elkin1*$^{-/-}$ mice also showed no deficits in open field locomotion (Fig S3E).

Sensory neuron mechanically-activated currents are lost in *Elkin1*$^{-/-}$ mice.

Large sensory neurons of the DRG are predominantly mechanoreceptors required for touch(*4*, *24*). We therefore recorded MA-currents from isolated sensory neurons evoked by mechanical indentation and substrate deflection (Fig 3A, D)(*24*, *25*). Normally, almost all large neurons exhibit robust predominantly RA MA-currents to both cell indentation and substrate deflection,(*14*, *25*) which we confirmed here in WT animals (Fig. 3A-F). However, only half of the large neurons (diameter >30 µm, Fig. S4A) from *Elkin1*$^{-/-}$ mice displayed any MA-current (Fig 3B,E). The insensitivity to mechanical stimuli was therefore concomitant to a loss of RA MA-currents in *Elkin1*$^{-/-}$ mice (Fig 3C, F). The current

amplitude of MA-currents in the remaining mechanosensitive neurons was similar in WT and *Elkin1*$^{-/-}$ mice, however, there was a small but significant (p = 0.01, unpaired Student's t-test) increase in the deflection threshold in neurons from *Elkin1*$^{-/-}$ mice as assessed through the pillar assay (Fig S4B,C). Large sensory neurons recorded from *Elkin1*$^{-/-}$ mice also showed a slightly depolarized resting membrane potential (p = 0.001, unpaired Student's t-test) consistent with the idea that this channel may contribute to membrane leak (Fig S4D). A significant loss of MA-currents was even detectable after loss of just one *Elkin1* allele (p = 0.005, unpaired Student's t-test) (Fig S4E). To show that the loss of MA-currents was not due to indirect effects of *Elkin1* gene inactivation, we conducted an acute rescue experiment. Using an adeno-associated virus neurotropic for sensory neurons (AAV-PHP.S-*hSyn-dtom-mElkin1*) we reintroduced *Elkin1* back into acutely isolated sensory neurons from *Elkin1*$^{-/-}$ mice. ELKIN1 protein was detected in infected sensory neurons from *Elkin1*$^{-/-}$ mice and there was a significant (p = 0.01, chi-sq test) rescue of MA-currents - just 40% neurons had MA-currents in mock transfected cells compared to 75% of cells 48 hours after infection with AAV-PHP.S-*hSyn-dtom-mElkin1* (Fig. 3G,H, Fig S5A).

Mechanically-activated currents in human sensory neurons depend on *ELKIN1.*

Human stem cells can be differentiated into sensory neuron-like cells which have characteristic electrophysiological properties of DRG neurons, including MA-currents (*26*, *27*). We could detect ELKIN1 protein in *NEUROGENIN2*-induced human sensory neurons (*26*) the staining for which was abolished by siRNA mediated knockdown of *ELKIN1*(Fig 3I and Fig S6A). Our induced human sensory neurons also possessed robust MA-currents which increased in size with increasing indentation amplitudes. MA-currents required higher indentation amplitudes and attained much smaller peak amplitudes in induced sensory neurons transfected with *ELKIN1* siRNA, compared to control scrambled siRNA (Fig 3I and Fig S6B,C). Thus, ELKIN1 is required for normal MA-current expression in both mouse and human sensory neurons. Additionally, in these induced human sensory neurons knockdown of *PIEZO2* using siRNA also decreased MA-currents and very little MA-currents remained after the knockdown of both *ELKIN1* and *PIEZO2* (Fig S6C). We therefore postulated that there may be some functional interaction between PIEZO2 and ELKIN1.

ELKIN1 and PIEZO2 share roles in sensory mechanotransduction.

The phenotype we observed in *Elkin1*$^{-/-}$ sensory neurons was similar to the knockdown or genetic ablation of the PIEZO2 mechanosensitive ion channel (*5*, *7*, *28*). Using smFISH we detected colocalization of *Elkin1* and *Piezo2* mRNA in WT DRG neurons, but no change in *Piezo2* mRNA expression was observed in *Elkin1*$^{-/-}$ sensory neurons (Fig S5B). Thus, *Elkin1* ablation does not affect *Piezo2* expression. As shown previously (*5*), we found that in WT DRG neurons, siRNA mediated knockdown of *Piezo2* approximately halved the number of neurons with MA-currents (Fig S5C). If *Elkin1* exerts its function via *Piezo2*, knockdown of *Piezo2* in *Elkin1*$^{-/-}$ neurons should not cause a further decrease in MA-currents. In contrast, our results show that MA-currents in *Elkin1*$^{-/-}$ neurons could be reduced further following *Piezo2* knockdown (Fig S5C). Thus, neurons retaining MA-currents in *Elkin1*$^{-/-}$ mice appear to have predominantly PIEZO2-dependent MA-currents. We next asked if there is a functional interaction between these two proteins by expressing *Piezo2* or *Piezo2* and *Elkin1* in N2a$^{Piezo1-/-}$ cells. We found no differences in the amplitude or kinetics of MA-currents found in single and double transfected cells indicating no substantial functional interaction between these proteins in a heterologous expression system (Fig S5D).

A known PIEZO2 modulator is the MEC-2-related mechanotransduction protein STOML3 which was shown to sensitize PIEZO2 channels to substrate deflection(*14*, *24*, *29*, *30*). We next asked whether there is also a molecular interaction between STOML3 and ELKIN1. Using a tripartite-GFP based protein complementation assay, we observed a robust green fluorescent signal indicating close association between STOML3 and ELKIN1 (Fig S7A). The protein complementation signal for a STOML3/ELKIN1 interaction was also blocked in the presence of the STOML3 oligomerization blocker OB1 (Fig S7A)(*30*). Co-expression of *Stoml3* with *Elkin1* in HEK293T$^{Piezo1-/-}$ cells revealed that ELKIN1-dependent MA-currents displayed decreased mechanical thresholds and increased current amplitude in the presence of STOML3 (Fig S7B).

Severe mechanoreceptor deficits in *Elkin1*$^{-/-}$ mice.

We next investigated whether ELKIN1 is required for the mechanosensory function of identified mouse mechanoreceptors. First, we used an ex vivo saphenous skin nerve preparation to trace the trajectory of single-units using an electrical stimulus until the point

of exit from the nerve branch. Using a mechanical stimulus we then searched for the mechanosensitive receptive field of the same unit which was usually located close the of exit point from the nerve branch (*6*, *7*, *24*, *31*). Normally, single identified Aβ-fibers with the fastest conduction velocities (>10 m/s) always have a mechanosensitive receptive field as confirmed here for WT mice (Fig. 4A). However, blinded recordings made from *Elkin1*$^{-/-}$ mice revealed that 40% of the Aβ-fibers had no detectable mechanosensitive receptive field (9/26 Aβ-fibers) (Fig 4A). Next, we examined the stimulus response properties of the remaining identified mechanoreceptors in the hairy skin. Aβ-fiber LTMRs innervating Merkel cells are classified as slowly-adapting mechanoreceptors (SAMs) with a dynamic and static response to ramp and hold force stimuli (Fig 4B). Normally around 50% of Aβ-fibers are classified as SAMs in the hairy skin(*24*, *32*) and this was the case here in both WT and *Elkin1*$^{-/-}$ mice (Fig S8A). However, the firing rates of SAMs to the static constant force phase of the stimulus was strongly reduced at all stimulus strengths in *Elkin1*$^{-/-}$ mice compared to controls (Fig 4B). Indeed, a plot of the peristimulus time histogram for SAMs stimulated with 150 mN of force reveals that firing rates decrease to almost zero just 3 seconds into a 10 second stimulus (Fig. 4C). However, the same SAMs from WT and *Elkin1*$^{-/-}$ mice showed similar dynamic phase responses (Fig S8C). The remaining Aβ-mechanoreceptors were classified as rapidly adapting mechanoreceptors (RAMs) which only respond to skin movement and code the velocity of skin movement(*3*, *4*, *33*). As a population, RAMs still coded the velocity of ramp stimuli, but the overall firing rates were significantly lower in *Elkin1*$^{-/-}$ mice compared to controls ($p = 0.03$, two-way ANOVA with multiple comparison) (Fig 4D). These results could easily reflect loss of MA-currents in mechanoreceptors, but could also be due to morphological disruption of sensory endings. However, an analysis of mechanoreceptor endings in the skin of *Elkin1*$^{-/-}$ mice did not reveal any obvious deficits (Fig S8C). These results show that around half of the LTMRs are insensitive to mechanical forces in *Elkin1*$^{-/-}$ mice, but in addition the remaining LTMRs showed profound functional deficits in their ability to detect mechanical force.

We also made recordings from single mechanosensitive nociceptors in the saphenous nerve. Sensory neurons with thinly myelinated Aδ axons can be classified as A-fiber mechanonociceptors (AMs) that signal fast pain(*34*) or D-hair receptors which are specialized LTMRs with directional sensitivity(*35*, *36*). We found no change in the

stimulus properties of D-hair or AM afferents in *Elkin1*$^{-/-}$ mice compared to controls (Fig. S8D). Many DRG with high amounts of ELKIN1 also appear to be nociceptors based on the presence of markers like IB4 and TRPV1(*22*). We thus made a focused analysis of MA-currents in small/medium diameter neurons that displayed broad humped action potentials characteristic of nociceptors(*22*, *25*, *37*) (Fig 5A, Fig S9). Many nociceptors in WT mice lack MA-currents to cell indentation (~40%)(*23*, *25*), but this was not different in neurons recorded from *Elkin1*$^{-/-}$ animals (Fig 5 A,B). However, when the MA-currents were classified as RA (rapidly adapting, inactivation time <10 ms), IA (intermediate adapting, inactivation time constant 10-50 ms) and SA (slowly-adapting, inactivation time constant >50 ms) we identified a significant ($p = 0.03$, chi-sq test) reduction in the proportion of RA MA-currents in *Elkin1*$^{-/-}$ mice compared to WT animals (Fig 5C). In addition, we found a small but significant ($p = 0.01$, unpaired Student's t-test) elevation in the amplitude of indentation needed to evoke the first MA-current in nociceptors from *Elkin1*$^{-/-}$ mice (Fig 5D). MA-currents evoked through substrate deflection showed no change between WT and *Elkin1*$^{-/-}$ mice (Fig S9B). We next focused our analysis on non-polymodal C-fibers that respond exclusively to mechanical stimuli and not to thermal stimuli as this population shows robust firing to mechanical force(*38*). In the ramp and hold force protocol, the firing of mechanosensitive C-fibers from *Elkin1*$^{-/-}$ mice was no different to that of WT animals (Fig 5E,F). We next analyzed the time course of C-fiber activation during a 10 s long constant force stimulus. Normally C-fibers show a moderate degree of adaptation during constant force stimuli(*7*). However, we found that even though initial firing rates were similar between genotypes at a stimulus strength of 100 mN firing rates dropped significantly ($p = 0.004$, two-way ANOVA with multiple comparison) more during the stimulus in C-fibers from *Elkin1*$^{-/-}$ mice (Fig. 5F,G Fig S10). Indeed, reduced firing rates towards the end of the stimulus were observed for all intensities of stimulation (Fig S10). Thus, unlike in mechanoreceptors, ELKIN1 has limited role in nociceptors, but may be necessary for maintaining sensitivity to constant forces in these neurons.

Discussion

Here we show that ELKIN1 is necessary for the mechanosensory function of most LTMRs. *Elkin1*$^{-/-}$ mice have electrically excitable sensory axons in the skin that were completely unable to respond to mechanical stimuli. The sustained firing of SAMs to constant force partly depends on PIEZO2 expressed in mechanosensory Merkel cells(*39*). Now our data suggest that ELKIN1 is required for the PIEZO2 independent transduction in SAMs as sustained responses were severely reduced in *Elkin1*$^{-/-}$ mice. Of note, the ability of induced human sensory neurons to transduce mechanical forces were severely diminished after knockdown of *ELKIN1*. Thus, ELKIN1 is an ion channel gated by mechanical force that likely has a conserved role in the transduction of light touch in mice and humans.

Consistent with the expression pattern of ELKIN1, we noted that maintained firing of C-fiber nociceptors to constant force was also impaired in the absence of the ELKIN1 protein. The loss of mechanically-gated currents, impaired touch-driven behavior and deficits in LTMR function are reminiscent of mice lacking *Stoml3* and of conditional *Piezo2* mutants (*7*, *24*, *28*, *40*). Our data supports a model where ELKIN1 and PIEZO2 channels share roles in sensory mechanotransduction in LTMRs, and that both can be modulated by STOML3. There is evidence that STOML3 can also modulate MA-currents in nociceptors consistent with a role for ELKIN1 in conferring robustness to the C-fiber responses to force(*14*). The identification of ELKIN1 as a mechanically gated-ion channel necessary for somatosensory function increases our understanding of the entirety of touch transduction.

References and Notes

1. A. R. Sobinov, S. J. Bensmaia, The neural mechanisms of manual dexterity. *Nat Rev Neurosci* **22**, 741–757 (2021).
2. M. Mikkelsen, E. L. Wodka, S. H. Mostofsky, N. A. J. Puts, Autism spectrum disorder in the scope of tactile processing. *Dev Cogn Neurosci* **29**, 140–150 (2018).
3. G. R. Lewin, R. Moshourab, Mechanosensation and pain. *J. Neurobiol.* **61**, 30–44 (2004).
4. S. G. Lechner, G. R. Lewin, Hairy sensation. *Physiology (Bethesda)* **28**, 142–150 (2013).
5. B. Coste, J. Mathur, M. Schmidt, T. J. Earley, S. Ranade, M. J. Petrus, A. E. Dubin, A. Patapoutian, Piezo1 and Piezo2 are essential components of distinct mechanically activated cation channels. *Science* **330**, 55–60 (2010).

6. S. S. Ranade, S.-H. Woo, A. E. Dubin, R. A. Moshourab, C. Wetzel, M. Petrus, J. Mathur, V. Bégay, B. Coste, J. Mainquist, A. J. Wilson, A. G. Francisco, K. Reddy, Z. Qiu, J. N. Wood, G. R. Lewin, A. Patapoutian, Piezo2 is the major transducer of mechanical forces for touch sensation in mice. *Nature* **516**, 121–125 (2014).

7. S. E. Murthy, M. C. Loud, I. Daou, K. L. Marshall, F. Schwaller, J. Kühnemund, A. G. Francisco, W. T. Keenan, A. E. Dubin, G. R. Lewin, A. Patapoutian, The mechanosensitive ion channel Piezo2 mediates sensitivity to mechanical pain in mice. *Science Translational Medicine* **10**, eaat9897 (2018).

8. B. U. Hoffman, Y. Baba, S. A. Lee, C.-K. Tong, E. E. Konofagou, E. A. Lumpkin, Focused ultrasound excites action potentials in mammalian peripheral neurons in part through the mechanically gated ion channel PIEZO2. *Proc Natl Acad Sci U S A* **119**, e2115821119 (2022).

9. A. Patkunarajah, J. H. Stear, M. Moroni, L. Schroeter, J. Blaszkiewicz, J. L. Tearle, C. D. Cox, C. Fuerst, O. Sanchez-Carranza, M. D. A. Ocana Fernandez, R. Fleischer, M. Eravci, C. Weise, B. Martinac, M. Biro, G. R. Lewin, K. Poole, TMEM87a/Elkin1, a component of a novel mechanoelectrical transduction pathway, modulates melanoma adhesion and migration. *eLife* **9** (2020).

10. C. M. Hoel, L. Zhang, S. G. Brohawn, Structure of the GOLD-domain seven-transmembrane helix protein family member TMEM87A. *Elife* **11**, e81704 (2022).

11. A. Han, A. Zhang, H. Kang, M. A. Maria-Solano, J. Yang, C. J. Lee, S. Choi, H. M. Kim, Structural insights into ion conduction by novel cation channel, TMEM87A, in Golgi apparatus. bioRxiv [Preprint] (2023). https://doi.org/10.1101/2023.01.03.522544.

12. A. E. Dubin, S. Murthy, A. H. Lewis, L. Brosse, S. M. Cahalan, J. Grandl, B. Coste, A. Patapoutian, Endogenous Piezo1 Can Confound Mechanically Activated Channel Identification and Characterization. *Neuron* **94**, 266-270.e3 (2017).

13. L.-Y. Chiang, K. Poole, B. E. Oliveira, N. Duarte, Y. A. B. Sierra, L. Bruckner-Tuderman, M. Koch, J. Hu, G. R. Lewin, Laminin-332 coordinates mechanotransduction and growth cone bifurcation in sensory neurons. *Nat. Neurosci.* **14**, 993–1000 (2011).

14. K. Poole, R. Herget, L. Lapatsina, H.-D. Ngo, G. R. Lewin, Tuning Piezo ion channels to detect molecular-scale movements relevant for fine touch. *Nat Commun* **5**, 3520 (2014).

15. L. Pope, M. Lolicato, D. L. Minor, Polynuclear Ruthenium Amines Inhibit K2P Channels via a “Finger in the Dam” Mechanism. *Cell Chemical Biology* **27**, 511-524.e4 (2020).

16. H. Kang, H. Jeong, A. Han, W. Koh, J. M. Lee, H. Jo, H. Lee, M. Bhalla, W. S. Roh, H. J. Jang, B. Lee, H. M. Kim, H. J. An, C. J. Lee, GolpHCat (TMEM87A): a unique voltage-gated and pH-sensitive cation channel in the Golgi. *bioRxiv*, 2023.01.03.522543 (2023).

17. D. Usoskin, A. Furlan, S. Islam, H. Abdo, P. Lönnerberg, D. Lou, J. Hjerling-Leffler, J. Haeggström, O. Kharchenko, P. V. Kharchenko, S. Linnarsson, P. Ernfors, Unbiased

classification of sensory neuron types by large-scale single-cell RNA sequencing. *Nature Neuroscience* **18**, 145–153 (2015).

18. N. Sharma, K. Flaherty, K. Lezgiyeva, D. E. Wagner, A. M. Klein, D. D. Ginty, The emergence of transcriptional identity in somatosensory neurons. *Nature* **577**, 392–398 (2020).

19. J. Kupari, D. Usoskin, M. Parisien, D. Lou, Y. Hu, M. Fatt, P. Lönnerberg, M. Spångberg, B. Eriksson, N. Barkas, P. V. Kharchenko, K. Loré, S. Khoury, L. Diatchenko, P. Ernfors, Single cell transcriptomics of primate sensory neurons identifies cell types associated with chronic pain. *Nat Commun* **12**, 1510 (2021).

20. H. Yu, D. Usoskin, S. S. Nagi, Y. Hu, J. Kupari, O. Bouchatta, S. L. Cranfill, Y. Su, Y. Lv, H. Song, G.-L. Ming, S. Prouty, J. Seykora, H. Wu, M. Ma, H. Olausson, P. Ernfors, W. Luo, Single-Soma Deep RNA sequencing of Human DRG Neurons Reveals Novel Molecular and Cellular Mechanisms Underlying Somatosensation. *bioRxiv*, 2023.03.17.533207 (2023).

21. P. Ray, A. Torck, L. Quigley, A. Wangzhou, M. Neiman, C. Rao, T. Lam, J.-Y. Kim, T. H. Kim, M. Q. Zhang, G. Dussor, T. J. Price, Comparative transcriptome profiling of the human and mouse dorsal root ganglia: an RNA-seq-based resource for pain and sensory neuroscience research. *Pain* **159**, 1325–1345 (2018).

22. C. L. Stucky, G. R. Lewin, Isolectin B(4)-positive and -negative nociceptors are functionally distinct. *J. Neurosci.* **19**, 6497–6505 (1999).

23. L. J. Drew, J. N. Wood, P. Cesare, Distinct Mechanosensitive Properties of Capsaicin-Sensitive and -Insensitive Sensory Neurons. *J. Neurosci.* **22**, 228RC (2002).

24. C. Wetzel, J. Hu, D. Riethmacher, A. Benckendorff, L. Harder, A. Eilers, R. Moshourab, A. Kozlenkov, D. Labuz, O. Caspani, B. Erdmann, H. Machelska, P. A. Heppenstall, G. R. Lewin, A stomatin-domain protein essential for touch sensation in the mouse. *Nature* **445**, 206–209 (2007).

25. J. Hu, G. R. Lewin, Mechanosensitive currents in the neurites of cultured mouse sensory neurones. *J. Physiol. (Lond.)* **577**, 815–828 (2006).

26. A. J. Hulme, J. R. McArthur, S. Maksour, S. Miellet, L. Ooi, D. J. Adams, R. K. Finol-Urdaneta, M. Dottori, Molecular and Functional Characterization of Neurogenin-2 Induced Human Sensory Neurons. *Frontiers in Cellular Neuroscience* **14** (2020).

27. K. Schrenk-Siemens, H. Wende, V. Prato, K. Song, C. Rostock, A. Loewer, J. Utikal, G. R. Lewin, S. G. Lechner, J. Siemens, PIEZO2 is required for mechanotransduction in human stem cell-derived touch receptors. *Nature neuroscience* **18**, 10–6 (2015).

28. S. S. Ranade, S.-H. Woo, A. E. Dubin, R. A. Moshourab, C. Wetzel, M. Petrus, J. Mathur, V. Bégay, B. Coste, J. Mainquist, A. J. Wilson, A. G. Francisco, K. Reddy, Z. Qiu, J. N. Wood, G. R. Lewin, A. Patapoutian, Piezo2 is the major transducer of mechanical forces for touch sensation in mice. *Nature* **516**, 121–125 (2014).

29. R. O'Hagan, M. Chalfie, M. B. Goodman, The MEC-4 DEG/ENaC channel of Caenorhabditis elegans touch receptor neurons transduces mechanical signals. *Nat. Neurosci* **8**, 43–50 (2005).

30. C. Wetzel, S. Pifferi, C. Picci, C. Gök, D. Hoffmann, K. K. Bali, A. Lampe, L. Lapatsina, R. Fleischer, E. S. J. Smith, V. Bégay, M. Moroni, L. Estebanez, J. Kühnemund, J. Walcher, E. Specker, M. Neuenschwander, J. P. von Kries, V. Haucke, R. Kuner, J. F. A. Poulet, J. Schmoranzer, K. Poole, G. R. Lewin, Small-molecule inhibition of STOML3 oligomerization reverses pathological mechanical hypersensitivity. *Nature Neuroscience* **20**, 209–218 (2017).

31. M. Kress, M. Koltzenburg, P. W. Reeh, H. O. Handwerker, Responsiveness and functional attributes of electrically localized terminals of cutaneous C-fibers in vivo and in vitro. *Journal of neurophysiology* **68**, 581–595 (1992).

32. M. Koltzenburg, C. L. Stucky, G. R. Lewin, Receptive properties of mouse sensory neurons innervating hairy skin. *J. Neurophysiol* **78**, 1841–1850 (1997).

33. F. Schwaller, V. Bégay, G. García-García, F. J. Taberner, R. Moshourab, B. McDonald, T. Docter, J. Kühnemund, J. Ojeda-Alonso, R. Paricio-Montesinos, S. G. Lechner, J. F. A. Poulet, J. M. Millan, G. R. Lewin, USH2A is a Meissner's corpuscle protein necessary for normal vibration sensing in mice and humans. *Nat Neurosci* **24**, 74–81 (2021).

34. A. Arcourt, L. Gorham, R. Dhandapani, V. Prato, F. J. Taberner, H. Wende, V. Gangadharan, C. Birchmeier, P. A. Heppenstall, S. G. Lechner, Touch Receptor-Derived Sensory Information Alleviates Acute Pain Signaling and Fine-Tunes Nociceptive Reflex Coordination. *Neuron* **93**, 179–193 (2017).

35. J. Walcher, J. Ojeda-Alonso, J. Haseleu, M. K. Oosthuizen, A. H. Rowe, N. C. Bennett, G. R. Lewin, Specialized mechanoreceptor systems in rodent glabrous skin. *The Journal of Physiology* **596**, 4995–5016 (2018).

36. M. Rutlin, C.-Y. Ho, V. E. Abraira, C. Cassidy, C. J. Woodbury, D. D. Ginty, The Cellular and Molecular Basis of Direction Selectivity of Aδ-LTMRs. *Cell* **159**, 1640–1651 (2014).

37. H. R. Koerber, R. E. Druzinsky, L. M. Mendell, Properties of somata of spinal dorsal root ganglion cells differ according to peripheral receptor innervated. *Journal of Neurophysiology* **60**, 1584–1596 (1988).

38. N. Milenkovic, C. Wetzel, R. Moshourab, G. R. Lewin, Speed and temperature dependences of mechanotransduction in afferent fibers recorded from the mouse saphenous nerve. *J. Neurophysiol.* **100**, 2771–2783 (2008).

39. S.-H. Woo, S. Ranade, A. D. Weyer, A. E. Dubin, Y. Baba, Z. Qiu, M. Petrus, T. Miyamoto, K. Reddy, E. A. Lumpkin, C. L. Stucky, A. Patapoutian, Piezo2 is required for Merkel-cell mechanotransduction. *Nature* **509**, 622–626 (2014).

40. M. Huang, G. Gu, E. L. Ferguson, M. Chalfie, A stomatin-like protein necessary for mechanosensation in C. elegans. *Nature* **378**, 292–295 (1995).

41. S. R. Chaplan, F. W. Bach, J. W. Pogrel, J. M. Chung, T. L. Yaksh, Quantitative assessment of tactile allodynia in the rat paw. *Journal of Neuroscience Methods* **53**, 55–63 (1994).

42. R. Gonzalez-Cano, B. Boivin, D. Bullock, L. Cornelissen, N. Andrews, M. Costigan, Up–Down Reader: An Open Source Program for Efficiently Processing 50% von Frey Thresholds. *Frontiers in Pharmacology* **9**, 433 (2018).

43. R. Dhandapani, C. M. Arokiaraj, F. J. Taberner, P. Pacifico, S. Raja, L. Nocchi, C. Portulano, F. Franciosa, M. Maffei, A. F. Hussain, F. de Castro Reis, L. Reymond, E. Perlas, S. Garcovich, S. Barth, K. Johnsson, S. G. Lechner, P. A. Heppenstall, Control of mechanical pain hypersensitivity in mice through ligand-targeted photoablation of TrkB-positive sensory neurons. *Nature communications* **9**, 1640–1640 (2018).

44. A. Zaimi, M. Wabartha, V. Herman, P.-L. Antonsanti, C. S. Perone, J. Cohen-Adad, AxonDeepSeg: automatic axon and myelin segmentation from microscopy data using convolutional neural networks. *Scientific Reports* **8**, 3816 (2018).

45. S. Cabantous, H. B. Nguyen, J.-D. Pedelacq, F. Koraïchi, A. Chaudhary, K. Ganguly, M. A. Lockard, G. Favre, T. C. Terwilliger, G. S. Waldo, A New Protein-Protein Interaction Sensor Based on Tripartite Split-GFP Association. *Scientific Reports* **3**, 2854 (2013).

Acknowledgments:

We thank Franziska Bartelt and Letizia Dalmasso for help with mouse genotyping, Bettina Purfürst for electron microscopy. We thank James Poulet, Stefan Lechner and members of the Lewin lab for constructive comments on the manuscript. The H9 cell line (WA09) used in this study is available under a material transfer agreement with WiCell.

Funding

This research was funded by an ERC grant Sensational Tethers 789128 to GRL, Deutsche Forschungsgemeinshaft CRC958 to AH and GRL and University of Wollongong and Friedreich's Ataxia Research Alliance/Association to MD.

SC and AR were recipients of Alexander von Humboldt research fellowships.

ATLH was a recipient of a Ministry of Science and Technology (Taiwan) fellowship (111-2917-I-564-011).

Author contributions:

Conceptualization SC and GRL

Mouse model design and validation GRL and VB

Patch clamp physiology and anatomy and cell biology SC with help from OCS, KP and ZMB.

Antibody validation CF, AH

Human induced sensory neurons and analyses AJH with help from RKFU, MD

Tripartite GFP design and implementation RF, AR and ATLH

Molecular biology ATLH.

Skin nerve electrophysiology JDK (nociceptors), MAK (mechanoreceptors, A-mechanonociceptors D-hair) and GRL (electrical search)

Behavioural assessment SC with help from TP, HH

Electron microscopy and analysis JDK and SC

Writing SC and GRL with input from all authors

Supervision and funding: GRL, AH, MD

Data and materials availability: All data are available in the manuscript or the supplementary materials. Prism files are available in Dryad doi:10.5061/dryad.0cfxpnw8s.

Competing Interests

The authors declare no conflict of interest

Supplementary Materials

Materials and Methods

Figs. S1 to S10

Tables S1 and S2

Figures

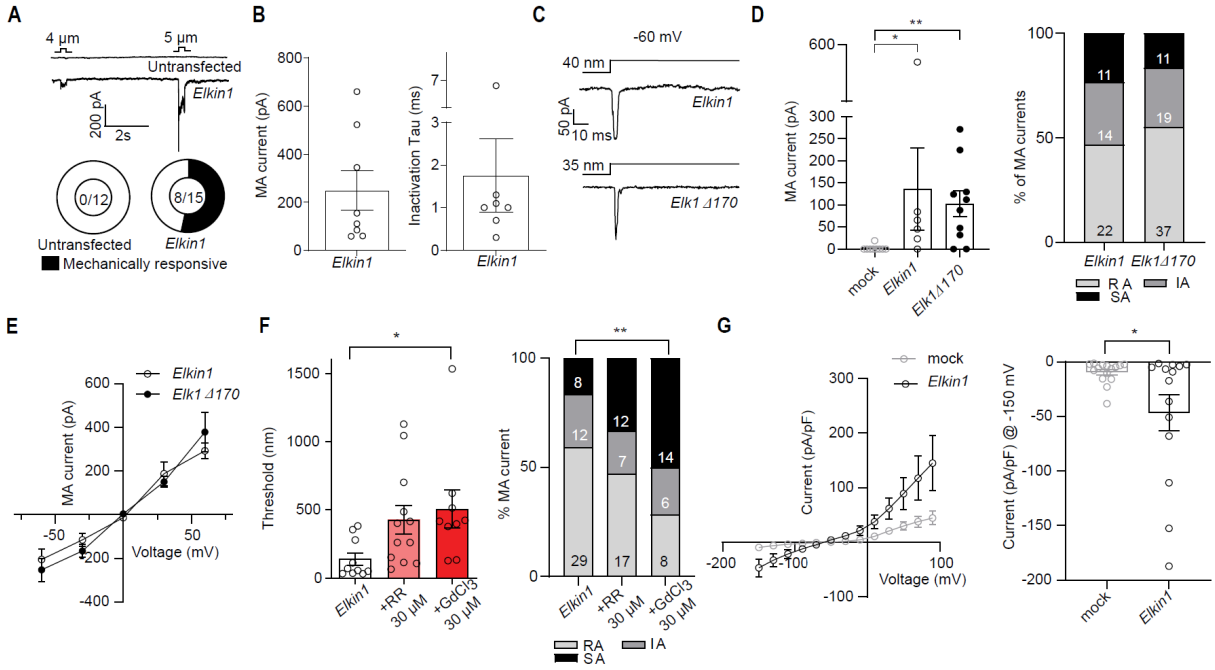

Figure 1: ELKIN1 forms a mechanically-gated channel. A. Pie chart shows total number of mechanically responsive transfected cells. **A**,**B.** Indentation-induced currents in HEK293T$^{Piezo1-/-}$ cells upon transfection with mouse *Elkin1* cDNA. Dots represent individual cells. **C.** Representative MA-currents evoked by pillar deflection at -60 mV along with **D**. Quantification of MA-current amplitude and properties at 100-250 nm force bin (each dot represents a cell and numbers in bars are number of MA pillar stimuli). **E.** Current-voltage relationship of MA-currents evoked in cells transfected with *Elkin1* or *Elk1Δ170*. Dots are mean of n=10 in *Elkin1* and n=15 in *Elk1Δ170* transfected cells. **F.** Quantification of pillar deflection threshold and properties of ELKIN1-dependent currents in the presence of pore blockers ruthenium red (RR) and $GdCl_3$. Each dot represents a cell and numbers in bars are number of MA pillar stimuli. **G.** Current-voltage relationship of *Elkin1* transfected cells (each dot is a mean of n=14 *mock* and n=15 *Elkin1* cells) as assessed through a series of voltage steps from -150 to 90 mV. Three group comparisons were made with one-way ANOVA followed by multiple comparison test and two group comparisons were made with Student's t-test. Proportions were compared using chi-squared test.* indicates $p < 0.05$, ** indicates $p < 0.01$. Error bars indicate SEM.

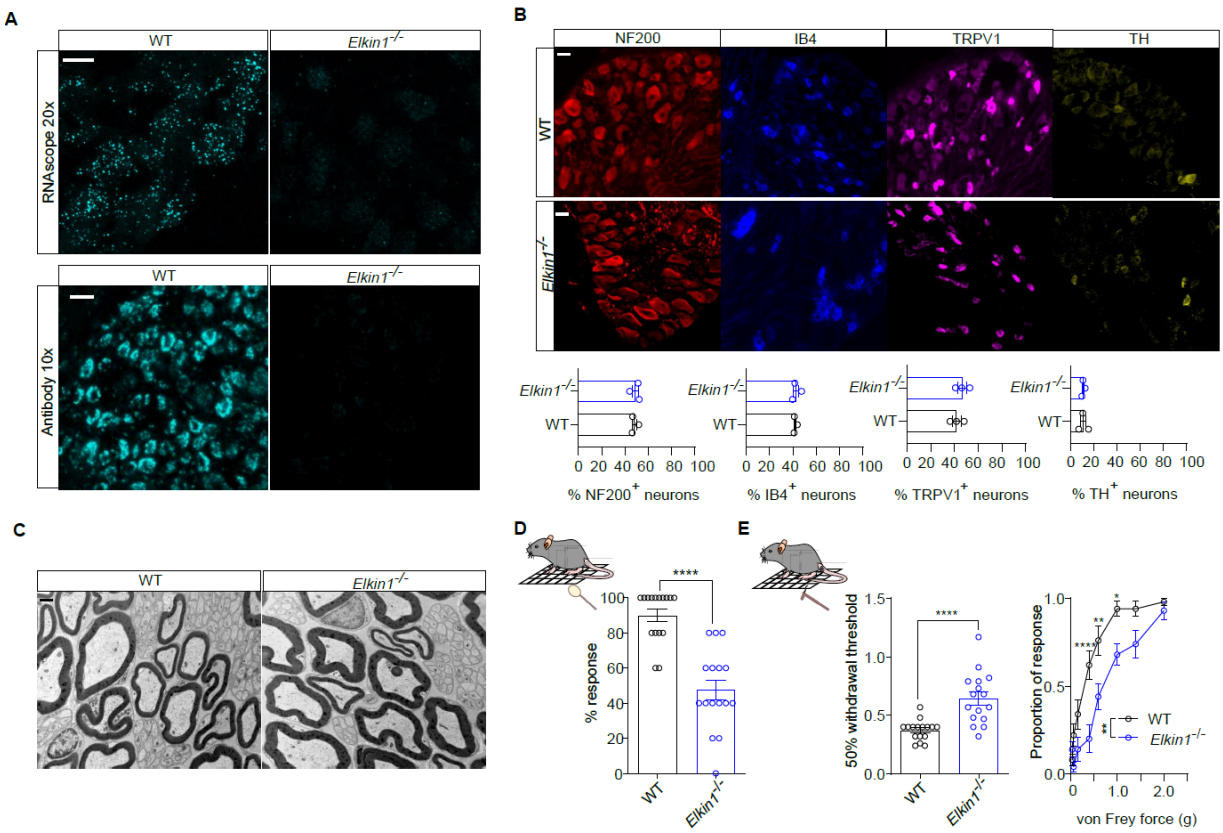

Figure 2: *Elkin1*$^{-/-}$ mice are touch insensitive. A. Representative images of ELKIN1 expression pattern, using a smFISH probe against *Elkin1* (top panel, scale = 20 μm) and antibody staining against ELKIN1 (bottom panel, scale = 50 μm) from WT and *Elkin1*$^{-/-}$ DRGs. **B.** Representative images of NF200 (red), IB4 (blue), TRPV1 (magenta) and TH (yellow) staining in WT and *Elkin1*$^{-/-}$ DRGs (top panel) and quantification of percent of positive neurons in each group from 3 male mice. >500 neurons counted in each category. **C.** Ultra-structural analysis of saphenous nerve. Scale bar = 1μm. **D:** Percent response of WT and *Elkin1*$^{-/-}$ mice (n=16) to brushing of a cotton swab. **E.** Paw withdrawal threshold (left, n=16) and ascending dose response (right, n=10) of WT and *Elkin1*$^{-/-}$ mice to von Frey filaments. Two group comparisons were made with Student's t-test and 2-way ANOVA with Sidak post hoc test (for von Frey ascending dose response). ** indicates $p < 0.01$, *** indicates $p < 0.001$. Error bars indicate SEM. Data from both male and female mice.

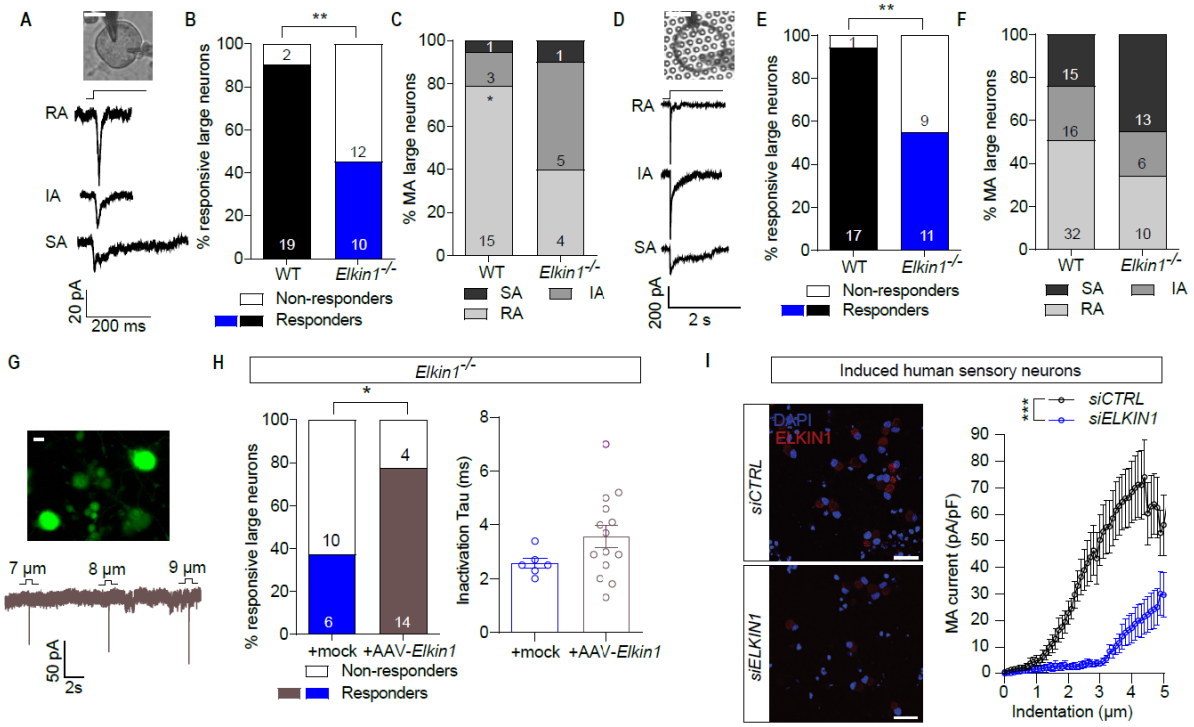

Figure 3: ELKIN1 is necessary and sufficient for mechanically-gated currents in mouse and human sensory neurons. **A.** Representative traces of currents generated by large diameter neurons from *Elkin1*$^{-/-}$ mice. Scale bar = 20 µm. **B.** Percent of large diameter neurons with an MA-current in WT and *Elkin1*$^{-/-}$ mice. **C.** Percent of rapidly, intermediate and slowly adapting, MA-currents in large diameter neurons. Number of cells are denoted in the bars. **D.** Representative traces of currents generated by pillar deflection of a large diameter neuron from an *Elkin1*$^{-/-}$ mouse. Scale bar = 20 µm. **E.** Percent of mechanically sensitive large diameter neurons in WT and *Elkin1*$^{-/-}$ mice in pillar assay. Number of cells are denoted in the bars. **F.** Percent of rapidly, intermediate and slowly adapting MA-currents in large diameter neurons. Number of MA pillar stimulations are denoted in the bars. **G.** top panel: Representative image of *Elkin1*$^{-/-}$ DRG neurons stained by anti-RFP after being transduced by AAV-PHP.S-*hSyn-dtom-mElkin1* (top panel, scale bar = 20 µm). **G**. bottom panel: Representative traces of indentation-induced currents from a transduced neuron. **H:** left panel: Percent of mechanically active large diameter neurons upon transduction with AAV-PHP.S-*hSyn-eGFP* (mock) or AAV-PHP.S-*hSyn-dtom-mElkin1*. **H.** Right panel: quantification of inactivation time constants of the measured currents. Each data point represents a single cell measured.
I. Representative images of *NEUROGENIN2* induced human sensory neurons before and after transfection with *ELKIN1* siRNA (left, scale = 50 µm; right, 2-way ANOVA). Proportions were compared using chi-sq test, four group comparisons were made using ANOVA followed by multiple comparison test. * indicates $p < 0.05$, ** indicates $p < 0.01$, *** indicates $p < 0.001$. Error bars indicate SEM. Data from both male and female mice.

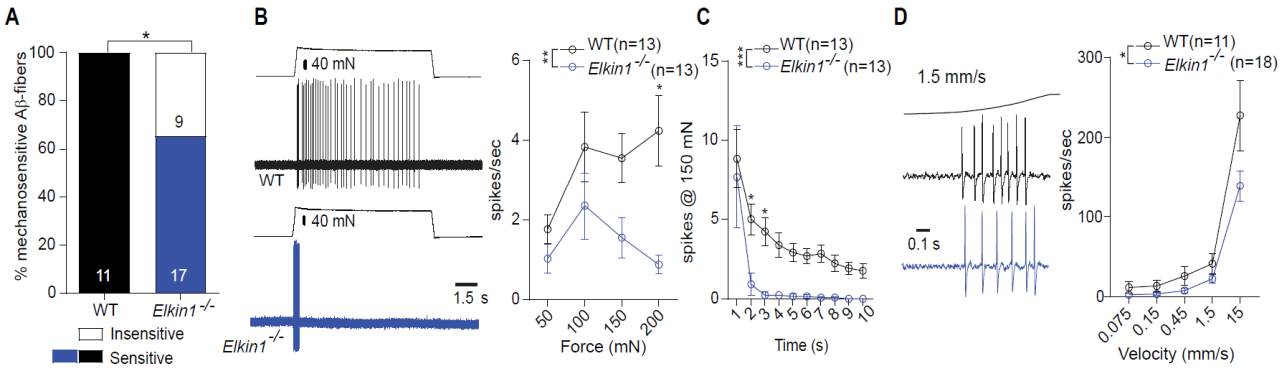

Figure 4 ELKIN1 is required for LTMR function. A. Percent of mechanosensitive fast conducting, Aβ-fibers in the saphenous nerve assessed with an electrical search protocol. **B.** Representative spikes evoked from slowly adapting mechanosensitive Aβ-fibers in WT and *Elkin1*$^{-/-}$ mice and quantification of mean spike rates with increasing force. **C.** Absolute number of spikes over a 10s time period in the 150 mN force bin (each dot represents average response from fibers). **D** Representative spikes evoked from rapidly-adapting mechanoreceptors to a moving ramp stimulus and quantification of the mean firing rates to ramps of increasing speed. Proportions were compared using chi-sq test (**A**.). All other group comparisons were made using 2-way ANOVA followed by multiple comparison. * indicates $p < 0.05$, ** indicates $p < 0.01$, *** indicates $p < 0.001$. Error bars indicate SEM. Data from both male and female mice.

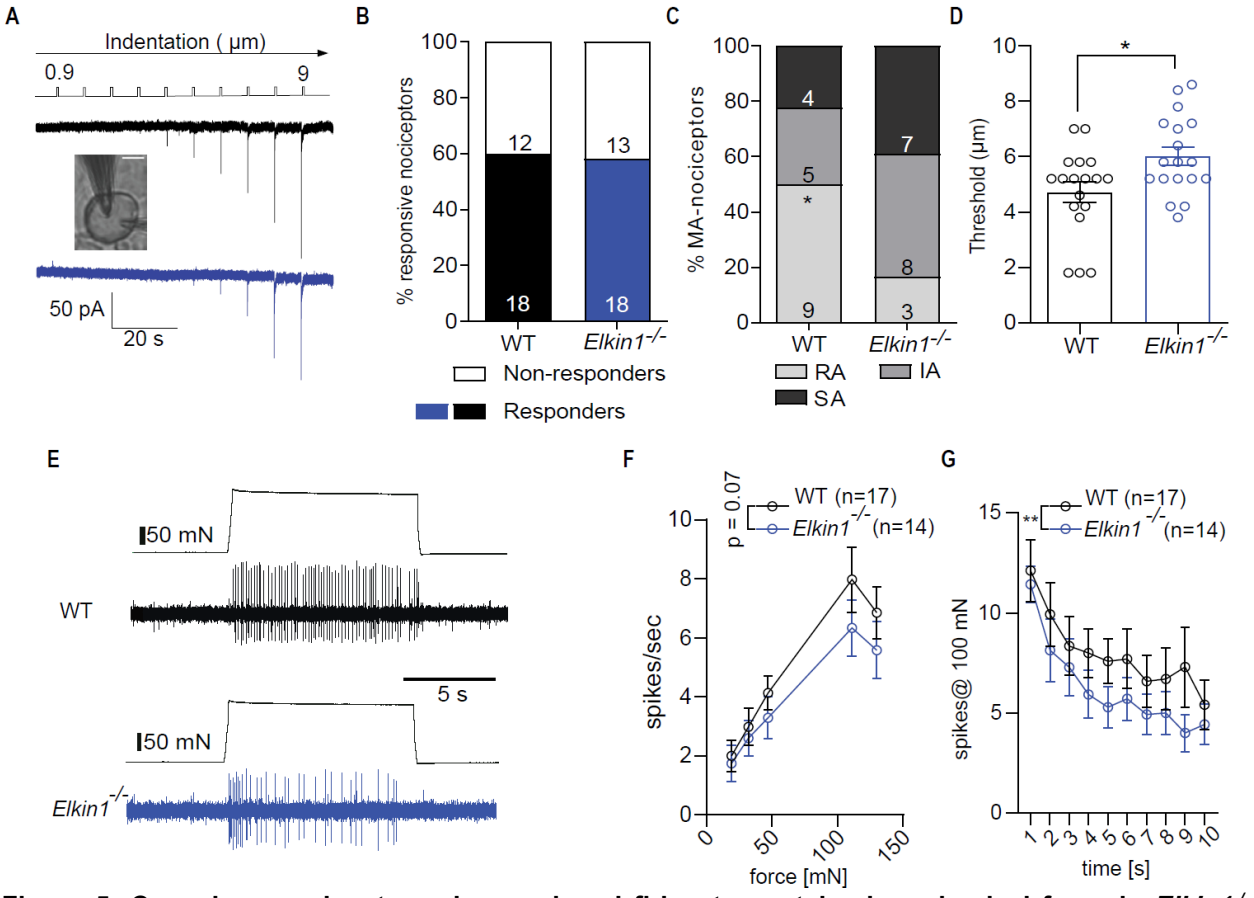

Figure 5: C-mechanonociceptors show reduced firing to sustained mechanical force in *Elkin1*$^{-/-}$ mice. A. Representative indentation-current evoked from WT and *Elkin1*$^{-/-}$ small DRG neurons. Scale = 20 µm. **B.** Percent of mechanically sensitive small/medium diameter neurons in WT and *Elkin1*$^{-/-}$ mice. **C.** Percent of rapidly, intermediate and slowly adapting MA-currents found in small/medium diameter neurons and their threshold for activation (**D**); the number of cells is denoted as dots in the bar graph. **E.** Representative spikes from mechanosensitive C-fibers in WT and *Elkin1*$^{-/-}$ mice. **F.** Quantification of the firing rates to increasing forces. **G.** Mean spiking rate over a 10s time period to a 100mN force stimulus. Dots in **F and G**. represent average of all fibers. Proportion was compared using chi-sq test. Two group comparison was made using Student's t-test. All other group comparisons were made using 2-way ANOVA followed by multiple comparison. * indicates $p < 0.05$, ** indicates $p < 0.01$, *** indicates $p < 0.001$. Error bars indicate SEM. Data from both male and female mice.

Science
AAAS

Touch sensation requires the mechanically-gated ion channel ELKIN1.

Authors

Sampurna Chakrabarti[1], Jasmin D. Klich[1], Mohammed A. Khallaf[1,2], Amy J. Hulme[3], Oscar Sánchez-Carranza[1], Zuzanna M. Baran[1,4], Alice Rossi[1], Angela Tzu-Lun Huang[1], Tobias Pohl[4], Raluca Fleischer[1], Carina Fürst[1,5], Annette Hammes[5], Valérie Bégay[1], Hanna Hörnberg[4,6], Rocio K. Finol-Urdaneta[3], Kate Poole[7], Mirella Dottori[3], Gary R. Lewin[1,8,9*]

Affiliations:

[1]Molecular Physiology of Somatic Sensation Laboratory, Max Delbrück Center for Molecular Medicine in the Helmholtz Association (MDC), Robert Rössle Str. 10, 13125 Berlin-Buch, Germany.

[2]Department of Zoology and Entomology, Faculty of Science, Assiut University, Assiut, 71516 Egypt

[3]School of Medical, Indigenous and Health Sciences, Molecular Horizons, University of Wollongong, Wollongong, NSW, 2522, Australia

[4]Molecular and Cellular Basis of Behavior, Max Delbrück Center for Molecular Medicine in the Helmholtz Association (MDC), Robert Rössle Str. 10, 13125 Berlin-Buch, Germany.

[5]Molecular Pathways in Cortical Development, Max Delbrück Center for Molecular Medicine in the Helmholtz Association (MDC), Robert Rössle Str. 10, 13125 Berlin-Buch, Germany.

[6]NeuroCure Cluster of Excellence, Humboldt-Universität zu Berlin, Unter den Linden 6, 10117 Berlin, Germany

[7]School of Biomedical Sciences, Faculty of Medicine & Health, University of New South Wales, Sydney, NSW 2052, Australia.

[8]Charité-Universitätsmedizin Berlin, Charitéplatz 1, 10117 Berlin, Germany

[9]German Center for Mental Health (DZPG), partner site Berlin.

[*]Correspondence to glewin@mdc-berlin.de

The PDF file includes:

Materials and Methods
Figs. S1 to S10
Tables S1 and S2

Materials and Methods

Animals

C57BL/6N adult (10-30 weeks) mice of both sexes were used in the study. Mice were housed in groups of 5 with food, water and enrichment available *ad libitum*. All animal protocols were regulated by the German federal authorities (State of Berlin). *Elkin1*$^{-/-}$ mouse line was generated by the Ingenious Targeting Laboratory (Ronkonkoma, NY) using CrispR/Cas9 strategy by deletion of exons 8 through 15 introducing a frameshift as illustrated in Fig S3A. The genotyping strategy utilized was as follows: For mutant genotyping: Forward primer: 5'- AAGGTGAAATAGCTCTCGATGG -3', reverse primer: 5'- GGGAAAGAACGGGAACACA -3' (expected band = 640 bp). For WT genotyping: Forward primer: 5' -TTTGCCAGTGACTGTTGAAGT – 3', Reverse primer: 5' -AGATAAAGGGGTCCCACAGGA – 3' (expected band = 481 bp). For experiments animals of different genotypes were chosen in a random manner based on availability.

Behavior

For all behavioral assays animals were habituated in the test paradigm for two days and analysis of the behaviors were carried out in a blinded manner (S.C. was aware of the group allocations).

Animals were placed on a raised platform with mesh-like floor (5x5 mm, von Frey apparatus) until they produced minimal movement. Paw withdrawal threshold was then assessed using a standard Semmes-Weinstein set of von Frey filaments (ranging from 0.07 - 2 g, Aesthesio) in accordance to the up-and-down method(*41*, *42*). 50 % paw withdrawal threshold was calculated using the open source software, Up-Down Reader (https://bioapps.shinyapps.io/von_frey_app/)(*42*). Ascending dose response with von Frey filaments were conducted by testing each filament 5 times and calculating the responses as proportions.

Withdrawal response to cotton swab was assessed as a measure of evoked responses to very small stimuli (0.7 – 1.6 mN(*43*)), while evoked responses to brush was used to measure intermediate touch sensation (>4 mN). For these tests, after habituation on the von Frey apparatus, a cotton swab (puffed out to ~ 3 times its original volume) or number 0 brush was applied in a sweeping motion across alternate hind paws, for a total of 5 times. The number of withdrawals throughout the trials was counted and coded as

percentage of total trials. A total of n=16 mice were used for von Frey, brush and cotton swab tests.

Hargreaves assay was used to assess the temperature sensitivity of mice. Briefly, mice were habituated on a plexiglass apparatus until minimal movement was observed. Their hind paws were then stimulated from below with an infrared light source (Ugo Basile, 37370) and the time required to withdraw the paws were recorded as indicators of their ability to assess temperature. N=6 mice were used Hargreaves test.

Male and female mice (n = 9) aged between 31-35 days were used to assess locomotor behaviour using the open field test. Testing was conducted during the inactive phase between 10 am and 3 pm. Before testing, the animals were habituated to the test room for at least 30 minutes.

The OFT apparatus consisted of an open arena (50x50 cm) where mice were allowed to freely explore for 10 minutes. Animal locomotion and location were recorded and tracked automatically using the ActiMot2 system (TSE Systems GmbH, Germany). Additionally, all trials were recorded using video cameras for subsequent detailed analyses. Between each trial, the arenas were cleaned using 80% ethanol and water and briefly dried with paper towels.

Sample sizes were determined using GPower 3.1 software based on previous studies. No animals were excluded from the analysis.

DRG neuron culture

Lumbar DRGs (L2-L5) were collected from mice into plating medium (DMEM-F12 (Gibco) supplemented with 10% fetal horse serum (FHS, Life Technologies) and 1% penicillin and streptomycin (P/S, Sigma-Aldrich)). These DRGs then underwent enzymatic digestion in 1.25% Collagenase IV (1 mg/ml, Sigma-Aldrich) for 1 hour at 37°C and 2.5% Trypsin (Sigma-Aldrich) for 15 min, at 37°C, followed by mechanical trituration with a P1000 pipette tip and purification in a 15% fraction V BSA column. The neurons were plated on glass bottomed plates (for indentation assays) or elastomeric pillar arrays (made as descried before(*14*)) coated with poly-L-lysine and laminin. Neurons were cultured overnight in an incubator (37°C and 5% CO2) and electrophysiological experiments were performed 18-24 hours after plating. For MA-current analysis (indentation) of large neurons n=4 WT, n=3 *Elkin1*$^{-/-}$ and n=3 *Elkin1*$^{+/-}$ animals were used.

For MA-current analysis of small neurons n=6 WT and n=6 *Elkin1*$^{-/-}$ animals were used. For pillar current analysis of large neurons n=6 WT and n=6 *Elkin1*$^{-/-}$ animals were used. Sample sizes were determined based on previous studies with similar effect sizes.

AAV transduction

AAV-PHP.S-*hSyn-dtom-mElkin1* (4.88 x 10^{12} vg/ml, canonical form of ELKIN1 Uniprot ID: Q8NBN3-1) and AAV-PHP.S-*hSyn-eGFP* (4.94 x 10^{12} vg/ml) were manufactured in the Charité Viral Core facility (Berlin, Germany). For viral transduction of DRG neurons, titre-matched amount of viruses were mixed with dissociated DRG neurons (after the mechanical trituration step described above) and plated on glass-bottomed dishes (50 µl per dish) coated with poly-L-lysine and laminin. Neurons were allowed to attach to plates for 2 hours before being submerged by plating medium. Some of the plated neurons were fixed and immunocytochemistry was performed using anti-TMEM87A (host: rabbit, HPA018104, 1:100) and anti-RFP (host: rabbit, AB34771, 1:500) antibodies to quantify percent of viral transduction. N=4 *Elkin1*$^{-/-}$ animals were used for this experiment.

siRNA transfection

2 hours after plating the DRG neurons in glass bottomed dishes, siRNA transfection was carried out using DharmaFECT (Horizon) reagents according to the manufacturers' guidelines. Briefly, siRNAs were mixed with serum and antibiotics free DRG neuron plating medium in a tube (total volume of 100 µl per dish), and 4.5 µl of DharmaFECT 4 transfection reagent was mixed with serum and antibiotics free DRG neuron plating medium (total volume of 100 ul) in another tube. Each tube was incubated separately for 5 min at RT, then mixed together and incubated for a further 20 min. 800 µl of antibiotics free complete medium was added to this mixture and added to the neurons. Experimental dishes were transfected with a final concentration of 50 nM ON-TARGETplus SMARTpool *mPiezo2* and 50 nM of siGLO green transfection indicator and control dishes were transfected with 50 nM of ON-TARGETplus Non-targeting Pool and 50 nM of siGLO green transfection indicator. Neurons were patched 48 hours after transfection with siRNA. N=4 WT and *Elkin1*$^{-/-}$ animals were used for this experiment.

Whole cell electrophysiology

Whole-cell patch clamp experiments were performed using heat-polished borosilicate glass pipettes (Harvard apparatus, 1.17 mm x 0.87 mm) with a resistance of 3-6 MΩ. The pipettes were pulled using a DMZ puller (Germany) and filled with a solution containing (in mM): 110 KCl, 10 NaCl, 1 $MgCl_2$, 1 EGTA and 10 HEPES, pH adjusted to 7.3 with KOH. Current-clamp experiments were performed to classify sensory neurons into mechano- and nociceptors. The extracellular solution contained (in mM): 140 NaCl, 4 KCl, 2 $CaCl_2$, 1 $MgCl_2$, 4 Glucose and 10 HEPES, pH adjusted to 7.4 with NaOH.

Currents were evoked either using pillar deflection or indentation of the soma at a holding potential of -60 mV. For pillar arrays experiments, a single pillar was deflected using a heat-polished borosilicate glass pipette (mechanical stimulator) driven by a MM3A micromanipulator (Kleindiek Nanotechnik, Germany) as described previously. Bright field images (Zeiss 200 inverted microscope) were collected using a 40X objective and a CoolSnapEZ camera (Photometrics, Tucson, AZ) before and after the pillar stimuli to calculate the pillar deflection. The light intensity of the center of each pillar before and after the stimuli was used to fit a 2D-Gaussian (Igor Software, WaveMetrics, USA) in order to calculate the pillar displacement. For mechanosensitive current-voltage curve with HEK293T$^{Piezo1-/-}$ cells, pillar displacements were produced at -60, -30, 0, 30 and 60 mV. For indentation experiments, indentation was produced on the neuronal cell membrane within the range of 1 – 9 µm using a heat-polished borosilicate glass pipette (mechanical stimulator) driven by a MM3A micromanipulator. For experiments with antagonists, cells were bathed in 30 µm ruthenium red (Sigma, 557450, diluted in ECS from a stock of 10 mM in water) and 30 µm $GdCl_3$ (Tocris, 4741, diluted in ECS from a stock of 100 mM in water). For cell-attached recordings, cells were subjected to four 20 mm of Hg pressure pulses using a high-speed pressure clamp instrument (ALA Scientific) for 500 ms each (total of 2s) separated by 1s of baseline (total of 4.5s). During analysis, the events during the pressure pulses were multiplied by 2.25 to normalize them to baseline durations.

Currents and the biophysical parameters were analysed using FitMaster (HEKA, Elektronik GmbH, Germany).

Induced human sensory neurons

Sensory neurons were generated via the induced expression of *NEUROGENIN-2 (NGN2)* in neural crest cells derived from H9 (WA09; WiCell) human pluripotent stem cells (*26*).

Mature induced sensory neurons were transiently transfected with either 1 μM control non-targeting siRNA (DHA-D-001910-01-20, Accell™, Horizon Discovery group), 1 μM *TMEM87A* (*ELKIN1*) siRNA (E-018401-00-0020, Accell™) and/or 1 μM *PIEZO2* (Pz2) siRNA (E-013925-00-0050, Accell™) for 96 hours (as described above). These induced sensory neurons were whole-cell patch clamped under voltage-clamp conditions (described above) and mechanically stimulated by fine probe indentation to the soma by increasing 0.1 μm steps (0.1 – 5 μm). Data is presented as mean ± SEM of the mechanically activated current normalized to the whole-cell capacitance (pA/pF) obtained from two independent differentiation/knockdown experiments.

Ex vivo skin nerve

Ex vivo skin nerve electrophysiology from cutaneous sensory fibers of the saphenous nerve was conducted following the method previously described(*35*). Briefly, mice were euthanized by CO_2 inhalation for 2-5 min followed by cervical dislocation, and the hair of the limb was shaved off. The hairy skin from the hind paw was removed along with the saphenous nerve up to the hip.

The innervated hairy skin was transferred to a bath chamber which was constantly perfused with warm (32°C) carbonated (95% O2, 5% CO2) interstitial fluid (SIF buffer): 123 mM NaCl, 3.5 mM KCl, 0.7mM MgSO4, 1.7 mM NaH2PO4, 2.0 mM CaCl2, 9.5 mM sodium gluconate, 5.5 mM glucose, 7.5 mM sucrose and 10 mM HEPES (pH 7.4). The skin was pinned out and stretched, such that the inside of the skin could be stimulated using stimulator probes. The nerve was fed through a small opening to an adjacent chamber filled with the mineral oil, where fine filaments were teased from the nerve and placed on a silver wire recording electrode.

Mechanically sensitive units were first located using blunt stimuli applied with a glass rod. The spike pattern and the sensitivity to stimulus velocity were used to classify mechanoreceptors as previously described(*24*, *30*, *35*). The raw electrophysiological data were recorded using a Powerlab 4/30 system and Labchart 8 software with the spike-histogram extension supported by an oscilloscope for visual identification and later analysis. All mechanical responses analyzed were corrected for the latency delay between the electrical stimulus and the arrival of the action potential at the electrode. The conduction velocity (CV) was measured with the formula CV = distance/ time delay, in

which CVs > 10 ms^{-1} were classified as RAMs or SAMs (Aβ, <10 ms^{-1} as Aδ and <1.5 ms^{-1} as C-fibers).

Mechanically sensitive units were stimulated using a piezo actuator (Physik Instrumente (PI) GmbH & Co. KG, model P-841.60) connected to a force sensor with calibrated conversion factor of Volts to Millinewtons. Different mechanical stimulation protocols were used to identify and characterize the sensory afferents. All types of mechanoreceptors were tested with a vibrating stimulus with increasing amplitude and 20 Hz frequency. The force needed to evoke the first action potential was measured. Additionally, a ramp and hold step was used with constant force (100 mN) and repeated with varying probe movement velocity (0.075, 0.15, 0.45, 1.5, and 15 mm s^{-1}). Only the firing activity evoked during the dynamic phase was analyzed. SAM mechanoreceptors, Aδ mechanoreceptors, and nociceptors were tested mechanically with a constant ramp (1.5–2 mN ms^{-1}) and hold (10 seconds of static phase) stimulation. Force of increasing amplitude was applied in five consecutive indentations, spikes evoked during the static phase were analyzed. Experiments were carried out in a blinded manner (S.C. was aware of the group allocations). N=12 WT and *Elkin1*$^{-/-}$ animals were used for LTMR and electrical search analysis, whereas n=8 each of WT and *Elkin1*$^{-/-}$ animals were used for C-fiber analysis.

Cell line culture

HEK293T*Piezo1*$^{-/-}$ and N2a*Piezo1*$^{-/-}$ cells were used for characterization of the currents evoked by mElkin1. HEK293T$^{Piezo1-/-}$ were cultured in DMEM-Glutamax (Gibco, ThermoFisher Scientific) supplemented with 10% fetal bovine serum (FBS, PAN Biotech Gmbh) and 1% penicillin and streptomycin (P/S, Sigma-Aldrich). N2a*Piezo1*$^{-/-}$ cells were cultured in DMEM-Glutamax (Gibco, ThermoFisher Scientific) supplemented with 45% Opti-MEM (Gibco, ThermoFisher Scientific), 10% FBS and 1% P/S. HEK293T*Piezo1*$^{-/-}$ and N2a*Piezo1*$^{-/-}$ cells were transiently transfected with 4 µl FuGene6 per 100 µl of Opti-MEM with 1 µg of cDNA as per the manufacturer's instructions. Cells were maintained in serum free medium overnight in a 37°C and 5% CO2 incubator before electrophysiological recordings. Data were obtained from at least 3 transfections. Plasmids used for transfection in electrophysiological studies are as follows: *mPiezo2*-IRES-eGFP,

mElkin1-IRES-dtomato, *mElkin1*-IRES-eGFP, *mElkin1-Δ1-170*-IRES-eGFP, *mStoml3*-2A-tdTomato. All *mElkin1* are Uniprot ID: Q8NBN3-1.

Immunohistochemistry

L2–L5 DRG were collected from animals (WT n= 3 and *Elkin1*$^{-/-}$ n=3) and postfixed in Zamboni's fixative for 1 hour, followed by overnight incubation in 30% (w/v) sucrose (in PBS) at 4°C for cryoprotection. DRG were next embedded in Shandon M-1 Embedding Matrix (Thermo Fisher Scientific), snap frozen on dry ice and stored at −80 °C. Embedded DRG were sectioned (12 µm) using a Leica Cryostat (CM3000; Nussloch), mounted on Superfrost Plus microscope slides (Thermo Fisher Scientific) and stored at −80 °C until staining. During staining, slides were washed with PBS-tween and blocked in antibody diluent solution: 0.2% (v/v) Triton X-100, 5% (v/v) donkey serum and 1% (v/v) bovine serum albumin in PBS for 1 hour at room temperature before overnight incubation at 4 °C with primary antibodies. The following primary antibodies were used on DRG tissue slides: anti-Tmem87a (host: rabbit, HPA018104, 1:100), anti-tyrosine hydroxylase (TH, host: sheep, AB1542, 1:1000), anti-NF200 (host: chicken, AB72996, 1:1000), anti-Trpv1 (host: goat, SC14298, 1:200).

Slides were then washed three times using PBS-tween and incubated with the following species-specific conjugated secondary antibodies at 1:500 - Alexa Fluor 488 anti-rabbit (A21206), Alexa Fluor 568 anti-sheep (A21099), Alexa Fluor 568 anti-chicken (A11041), Alexa Fluor 555 anti-goat (A21432) or Isolectin GS B4 conjugated to Alexa 594 (121413, Thermo Fisher) for 2 hours at room temperature (20-22 °C). The secondary antibody was washed three times in PBS tween, mounted with Dako (Agilent, S3023) and imaged with a Leica fluorescent microscope. Exposure levels were kept constant for each slide and the same contrast enhancements were made to all slides. Negative controls without the primary antibody showed no staining with either secondary. DRGs from *Elkin1*$^{-/-}$ mice did not show staining with anti-TMEM87A antibody. Positive neurons were scored as using an R toolkit (https://github.com/amapruns/Immunohistochemistry_Analysis) followed by manual validation. Briefly, mean gray value (intensity) of all neurons in 1–3 sections from each DRG level of interest in each mouse was measured using ImageJ. A neuron was scored as positive for a stain if it had an intensity value >2 SDs above the average normalized minimum gray value across all sections.

Free-floating immunohistochemistry was conducted on 40 µm sections of hairy skin as described above with minor adjustments such as longer washes and incubation in primary antibodies (anti-NF200 (host: chicken, AB72996, 1:500), anti-S100B (host: rabbit, 15146-1-AP, 1:200) for 72 hours and in secondary antibodies (Alexa Fluor 488 anti-chicken, A11039, 1:500, Alexa Fluor 568 anti-rabbit, A10042, 1:500) overnight. The free-floating sections were then mounted on glass slides using 0.2% gelatine in PBS and imaged using a ZEISS confocal microscope.

SmFISH

Elkin1 and *Piezo2* mRNA levels were assessed in DRGs from WT (n = 3) and *Elkin1*$^{-/-}$ (n = 3) mice using RNAscope assay (a fluorescent in situ hybridization technology). Briefly, snap-frozen and embedded DRGs were sectioned and mounted on coverslips as described above. Next, hybridization of probes and subsequent signal development was carried out using H_2O_2 and Protease Reagents and Multiplex Fluorescent Detection Reagents v2 kits (Advanced Cell Diagnostics (ACD); Hayward, CA) as described in the manufacturer's protocol. The following probes were used: *Piezo2* - Mm-*Piezo2*-E43-E45 (C1 #439971) and *Elkin1* - Mm-*Tmem87a* (C3 #868581). The fluorophores applied to detect the signal from the probes were Opal 690 Reagent (1:750; Akoya Biosciences, #FP1497001KT) for C1 and Opal 570 Reagent (1:750; Akoya Biosciences, #FP1488001KT) for C3. Lastly, slides were incubated with RNAscope DAPI and cover slipped using Fluorescence Mounting Medium (Dako)

Electron microscopy

Saphenous nerves from WT (n=3) and *Elkin1*$^{-/-}$ (n=3) mice were examined using a Zeiss 910 electron microscope. Briefly, nerves were isolated and fixed in 4% paraformaldehyde/2.5% glutaraldehyde in 0.1 M phosphate buffer for at least 24 hours at 4°C, before being treated with 1% OsO4 for 2 hours and dehydrated in an ethanol gradient and propylene oxide. Then, the nerves were embedded in polyresin, cut using a microtome in ultrathin sections (70 nm) and imaged at 2500x magnification. Analysis of the A and C fibre dimensions were made(*44*) using https://axondeepseg.readthedocs.io/en/latest/ followed by manual quality control by a blinded experimenter (S.C. was aware of the group allocations).

Tripartite split-GFP complementation assay

The tripartite split-GFP complementation assay (modified from(*45*)) was performed in HEK293T (ACC 635, DSMZ). HEK293T cells were cultured in DMEM (DMEM 41966) supplemented with 10% FCS and 1% Penicillin/Streptomycin. HEK293T cells were cultured to about 70% confluence; cells were co-transfected, as indicated, with GFP1-9::iRFP702 (Addgene #130125), *mStoml3*- GFP10::mCHERRY and *mElkin1*-GFP11::eBP2 plasmids using Fugene HD and following manufacturer's instructions (Promega). Seven hours after transfection, the culture medium was changed with fresh medium containing DMSO or OB1 (5µM). After 40 hours, cells were fixed in 4% PFA and images (*eGFP*, *mCherry* and *eBFP2*) were acquired using a CytationC10 (Biotek, Objective 60x). *eGFP* (interaction signal) and *mCherry* (transfection control signal) percentage of cells and fluorescence intensity were analyzed using Gen5 (Biotek). *eGFP* signal was normalized with *mCherry* signal (% *eGFP*/*mCherry* and fluorescence intensity *eGFP*/*mCherry*), data were then normalized to control (DMSO).

Statistical analysis

All statistical tests used are detailed in the figure legends. Comparisons between two groups were carried out using Student's t-test and more than three groups using ANOVA with post hoc tests. Proportions were compared using the chi-sq test. Electrophysiological skin nerve data consisting of two groups and multiple time points/forces were compared using 2-way ANOVA. Steps were taken to ensure that control and experimental groups were spread across different days to reduce bias.

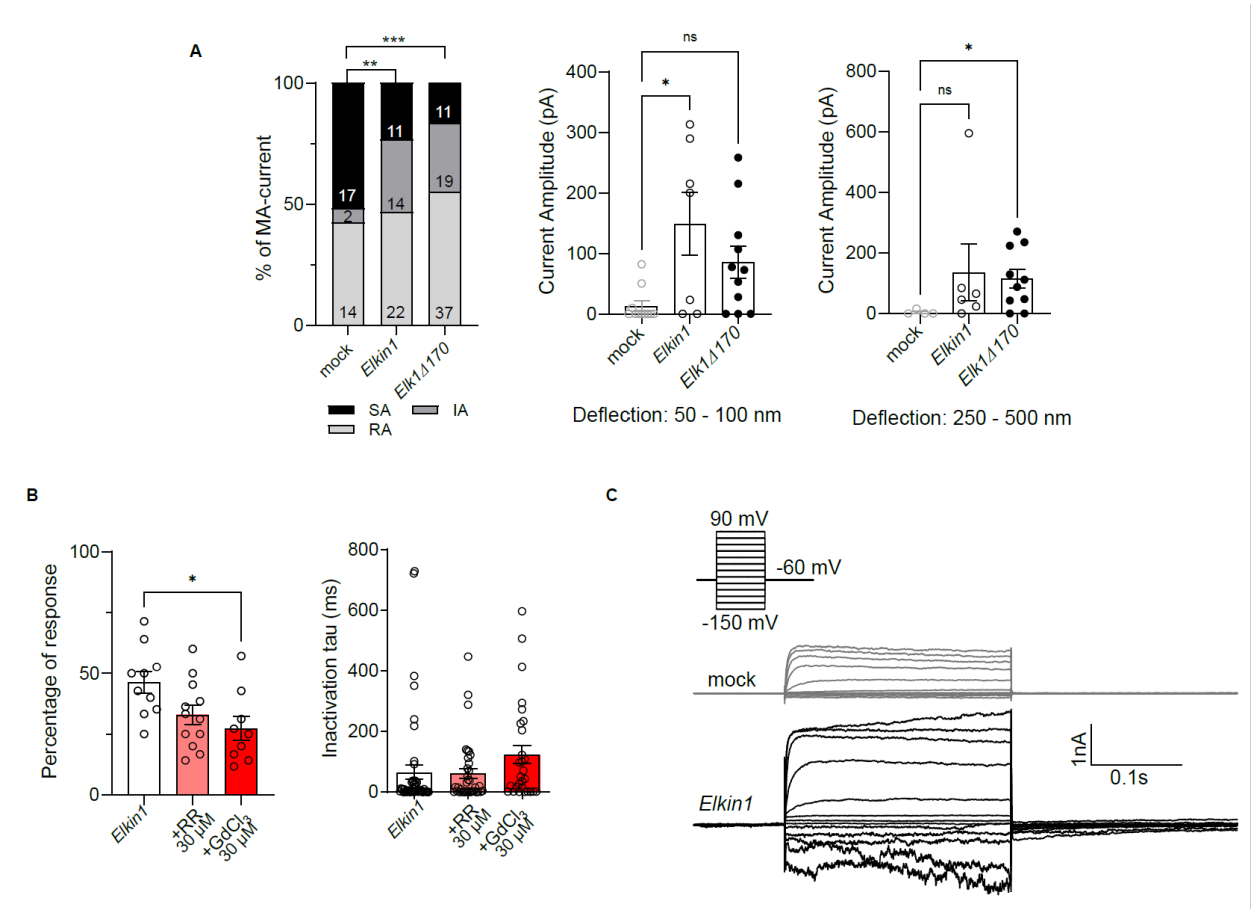

Fig S1: Biophysical properties of ELKIN1 currents. A) Left: percent of rapidly adapting (RA), intermediately adapting (IA) or slowly adapting (SA) MA-currents evoked by pillar assay (substrate deflection) in HEK293T$^{Piezo1-/-}$ cells. Numbers in bars represent number of deflections. Middle: amplitudes of MA-currents evoked at 50-100 nm and (right) 250-500 nm force bins. B) Percent of mechanically active pillar stimulations (each dot represents a cell) and their inactivation time constants (each dot represents a pillar stimulation) in *Elkin1* transfected HEK293T$^{Piezo1-/-}$ cells when incubated with either 30 μm ruthenium red (RR) or 30 μm $GdCl_3$. C) Raw traces of leak currents in mock (grey) and *Elkin1* (black) transfected HEK293T$^{Piezo1-/-}$ cells. Proportions were compared using chi-sq tests, three group comparisons were made using ANOVA followed by multiple comparison tests. * indicates $p < 0.05$, ** indicates $p < 0.01$, *** indicates $p < 0.001$. Error bars indicate SEM.

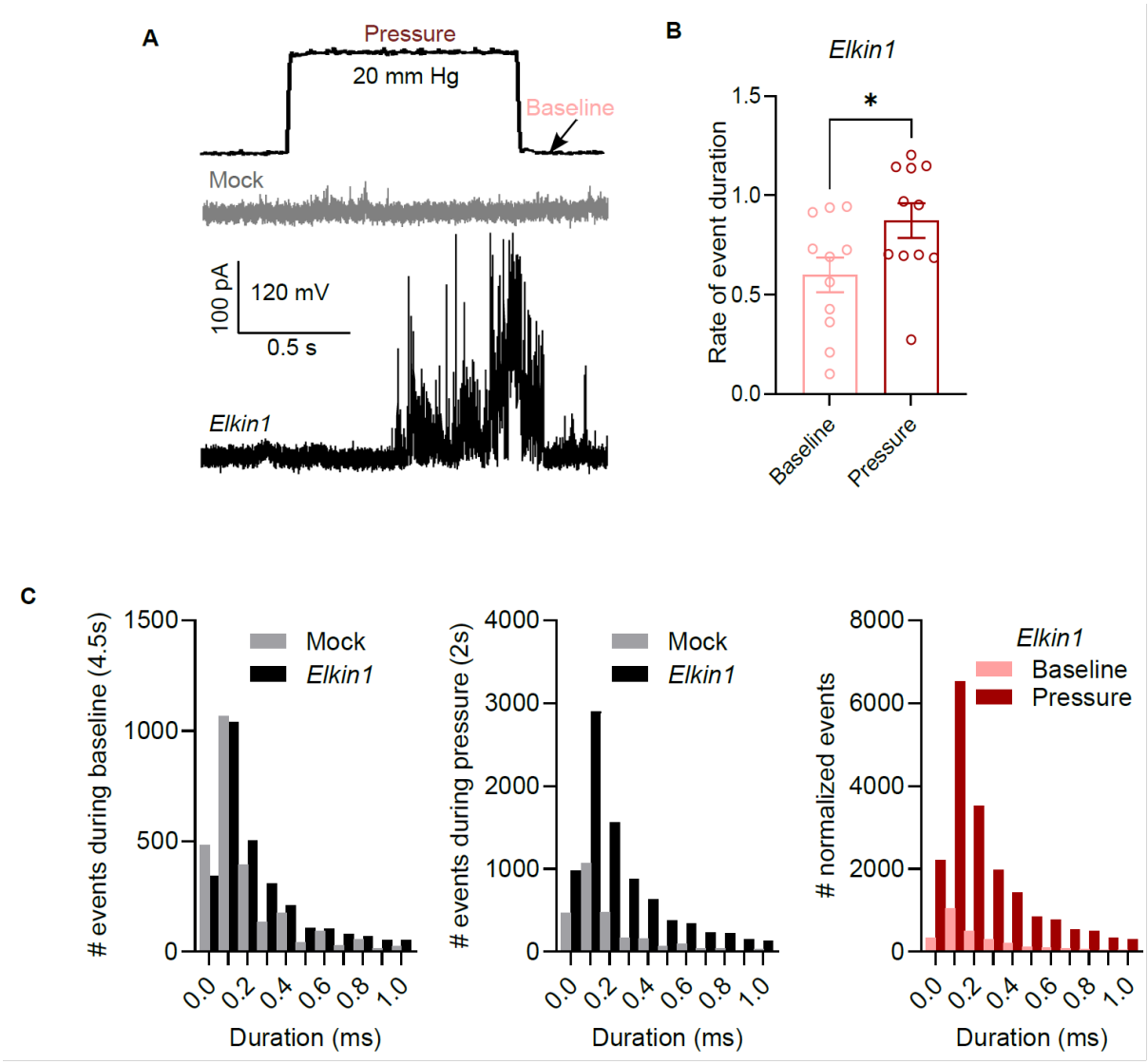

Fig S2: Cell-attached recordings of ELKIN1 detects low-pressure. A) Representative single-channel-like events in mock and *Elkin1* transfected HEK293T$^{Piezo1-/-}$ cells. B) Rate of summed total duration of events during pressure pulses vs. baseline in *Elkin1* transfected cells. C) Raw event count histograms in mock (grey) and *Elkin1* (black) transfected cells at baseline (left), during pressure (middle) as well as comparison of baseline (pink) and under pressure application (maroon) in *Elkin1* transfected cells. Error bars indicate SEM.

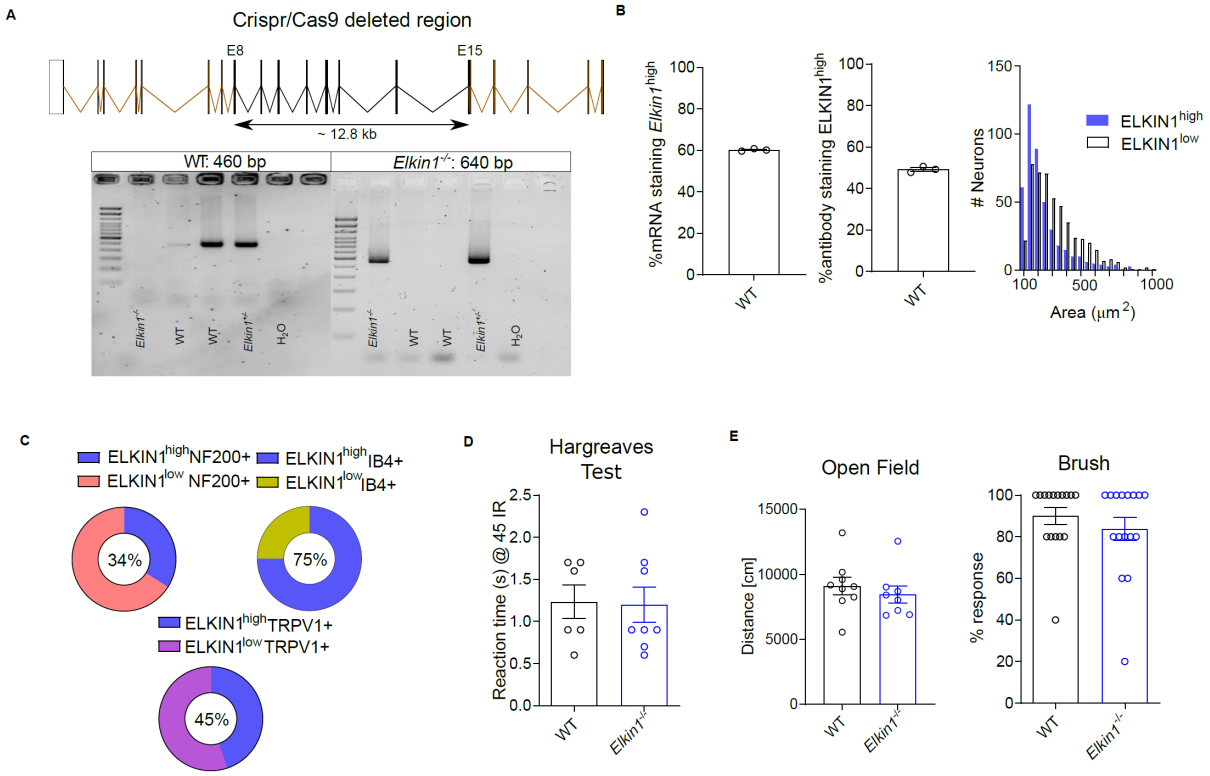

Fig S3: Characterization of *Elkin1*$^{-/-}$ mice using immunohistochemical and behavioral assays. A) Representation of the strategy to knockout *Elkin1* using Crispr/Cas9 along with PCR bands from genomic DNA of WT, *Elkin1*$^{+/-}$ and *Elkin1*$^{-/-}$ mice. B) Percent of DRG sensory neurons expressing high amounts of *Elkin1* as assessed through RNAscope (left) and immunohistochemistry (right). Dots represent each mouse, > 100 neurons were analyzed in each mouse; along with a distribution of cell body area. C) Quantification of colocalization between sensory neurons expressing high amounts of ELKIN1 and positive for NF200 (orange), IB4 (yellow) and TRPV1 (magenta). Number inside circles represent the highly expressing ELKIN1 group. D) Hargreaves assay for noxious thermal behavior in WT (n=6) and *Elkin1*$^{-/-}$ (n=8) mice. E) Open field test showing total distance travelled (WT n=9 and *Elkin1*$^{-/-}$ n=8) and brush test showing percent withdrawal upon brushing of the paw (WT n=16 *Elkin1*$^{-/-}$ n=16). Error bars indicate SEM.

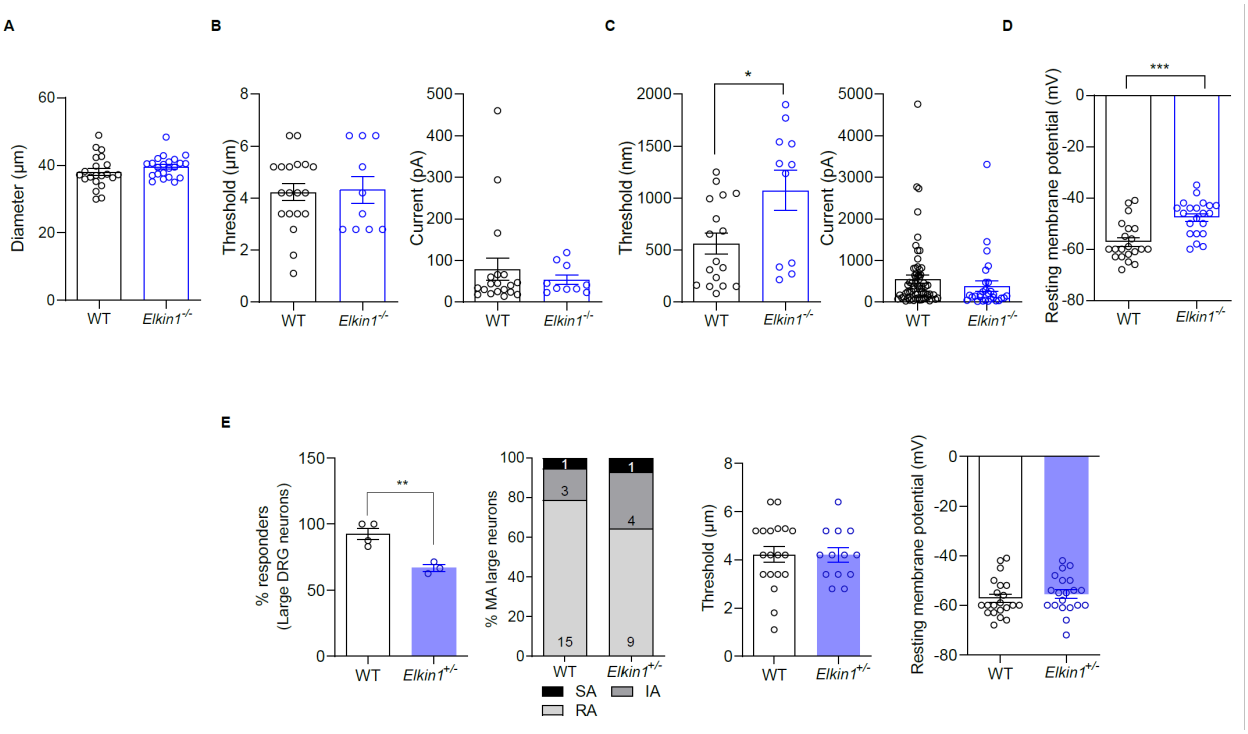

Fig S4: Electrophysiological properties of large diameter DRG neurons. A) Diameter of neurons recorded and classified as large diameter neurons. B) Threshold of MA-current activation in the indentation assay along with the maximal (max) amplitude of these currents. C) Threshold of MA-current activation in the pillar assay (each dot represents individual cells) along with the max amplitude of these currents (each dot represents individual stimulation). D) Resting membrane potential of large neurons. E) Properties of MA-currents in *Elkin1+/-* mice as assessed through indentation assay including percent MA, percent of rapidly (RA), intermediately (IA) or slowly adapting (SA) MA-currents, threshold of MA-current activation and resting membrane potential. WT data is the same used for comparison with *Elkin1*$^{-/-}$ mice. Data obtained from both male and female mice. Two groups were compared using two-sided Student's t-test. ** indicates $p < 0.01$, *** indicates $p < 0.001$. Error bars = SEM. Data obtained from n = 3 WT and n = 3 *Elkin1+/-* mice.

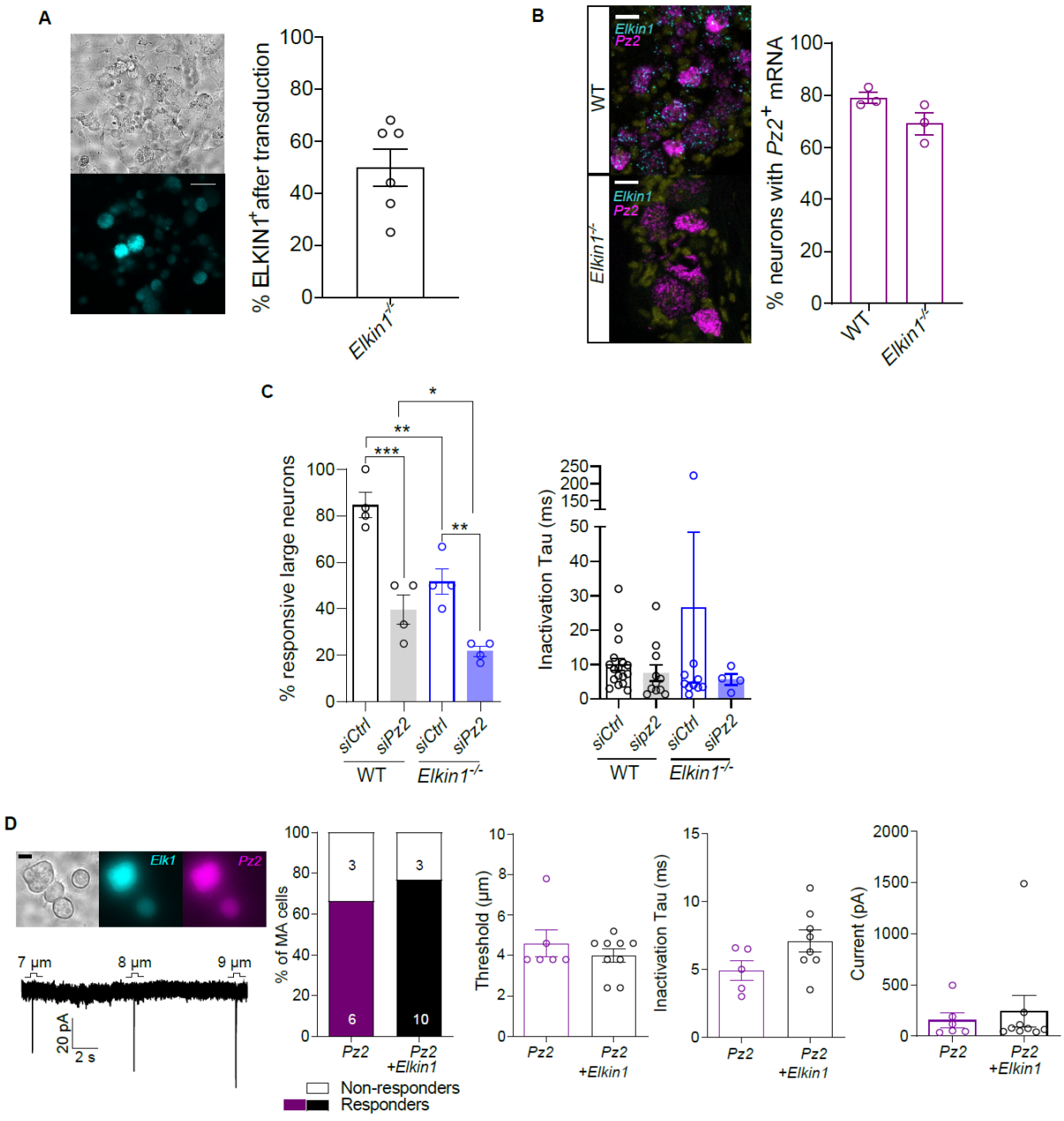

Fig S5: ELKIN1 replacement and colocalization with PIEZO2. A) Left: representative image of sensory neurons from *Elkin1*$^{-/-}$ mice transduced with AAV-PHP.S-*hSyn-dtom-mElkin1* and stained with anti-TMEM87A (ELKIN1) antibody. Scale = 100 µm. Right: quantification of the percent of ELKIN1 positive neurons after viral transduction. Dots represent 2 dishes each from 3 mice. B) percentage of DRG neurons positive for *Piezo2* mRNA as assessed through RNAscope along with representative images (left). Scale = 10 µm. C) left: Percentage of MA large neurons in WT or *Elkin*$^{-/-}$ mice transfected with Control scrambled (*siCtrl*) or *Piezo2* siRNA (*siPz2*). Each dot represents a mouse (number of neurons in each group is 20, 22, 19 and 19 respectively). right: inactivation time constants of currents measured in each group. D) N2a$^{Piezo1-/-}$ cells transfected with

Elkin1 and *Piezo2* cDNA showing similar percent of MA cells, threshold of MA-current inactivation time constant and peak current amplitude as assessed through indentation assay. Four group comparisons were made using ANOVA followed by multiple comparison test. * indicates $p < 0.05$, ** indicates $p < 0.01$, *** indicates $p < 0.001$. Error bars indicate SEM Data from both male and female mice.

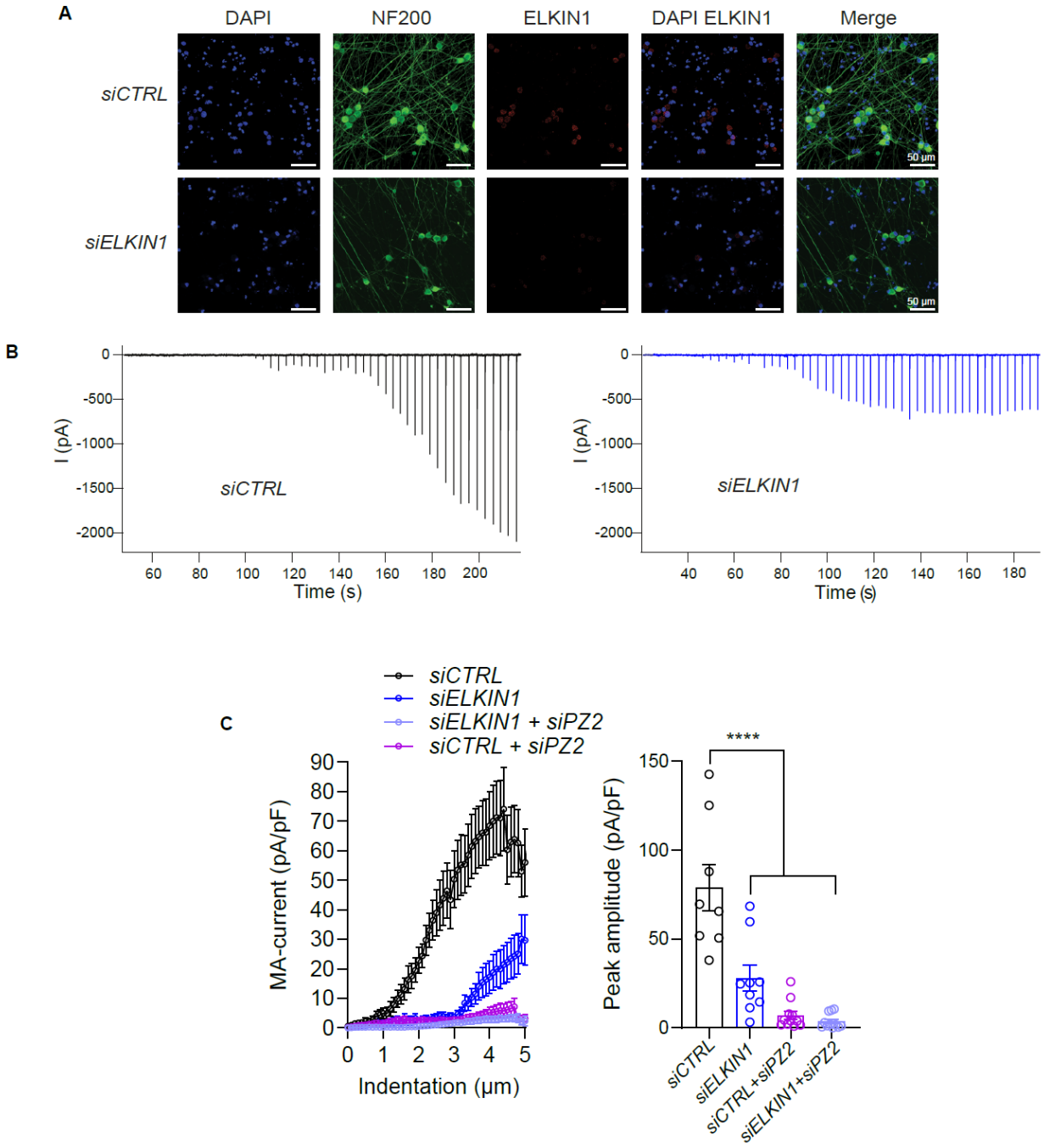

Fig S6: ELKIN1-mediated MA-currents in induced human sensory neuron. A) Representative image of *NEUROGENIN2* induced human sensory neurons stained with NF200 and ELKIN1 with or without siRNA mediated *ELKIN1* knockdown. Scale bar indicates 20 µm. B) Representative MA-current traces with or without siRNA mediated *ELKIN1* knockdown evoked by neuronal indentation. C) Quantification of the MA-currents after transfection with control siRNA or siRNAs against *ELKIN1*, *PIEZO2* or both showing decreasing peak amplitude across conditions. Comparisons were made using ANOVA **** indicates $p<0.0001$. Error bars indicate SEM.

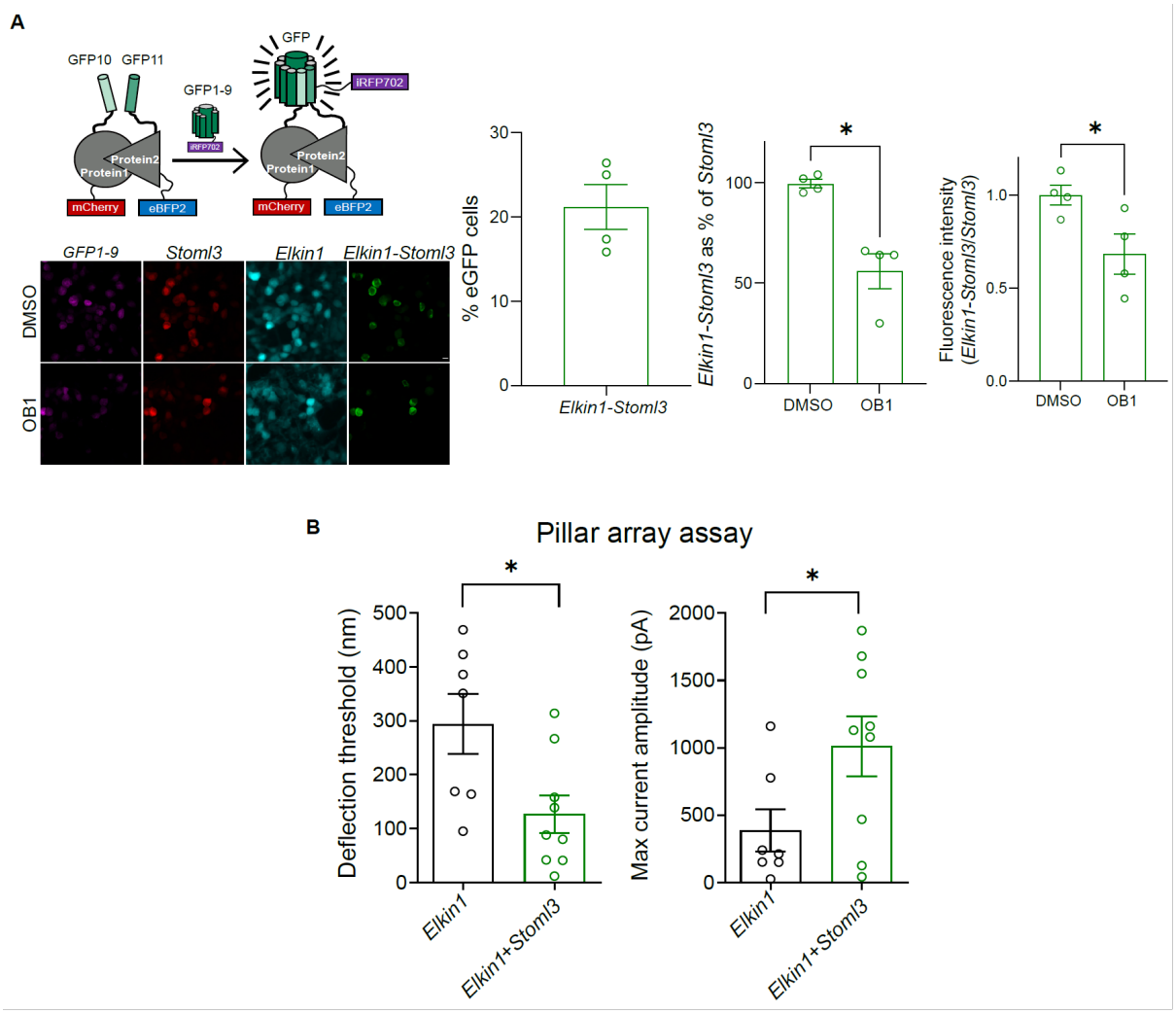

Fig S7: STOML3 interacts with ELKIN1. A) Tripartite GFP based protein complementation assay showing percent interaction of STOML3 and ELKIN1 (% eGFP cells) along with interaction when incubated with an antagonist of STOML3 oligomerization, OB1. B) Threshold of MA-current activation and peak MA-current amplitude evoked by pillar deflections in HEK293T$^{Piezo1-/-}$ cells transfected with *Elkin1* and *Elkin1+Stoml3*. Scale bar = 10 μm. Two groups were compared using two-sided Student's t-test. * indicates $p < 0.05$. Error bars indicate SEM

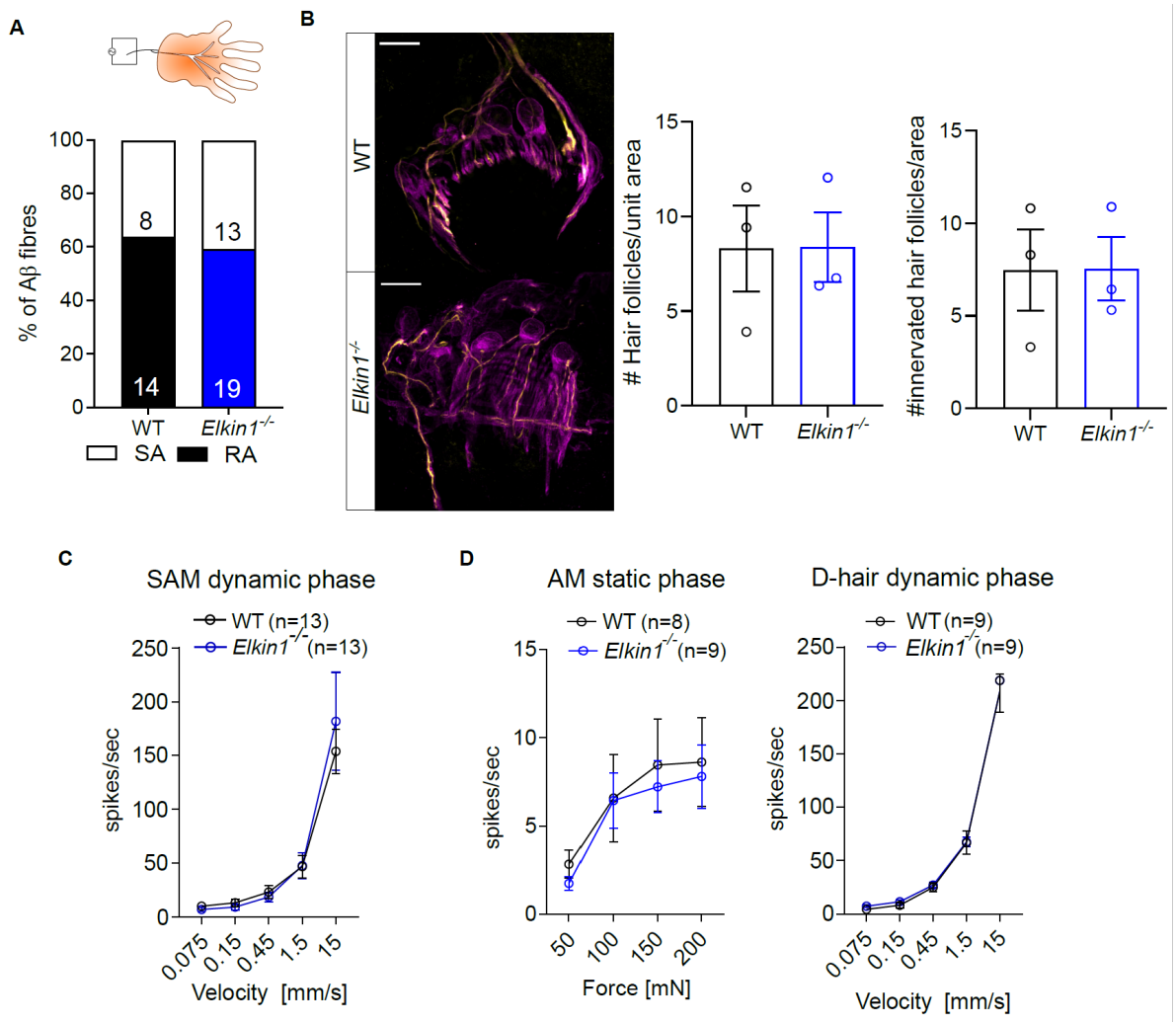

Fig S8: Characterization of saphenous nerve innervating the skin. A) percent of slowly adapting and rapidly adapting Aβ-fibers. B) representative images of fast conducting NF200 (yellow) positive nerve fibers innervating hair follicles marked by S100b (magenta) and quantification of hair follicles and innervated hair follicles in WT and *Elkin1*$^{-/-}$ mice. Scale bar = 50 μm. Each dot represents a mouse, at least 3 images were analyzed per mouse. C) mean spike rates of slowly adapting mechanosensitive Aβ-fibers in the dynamic phase (in response to ramps of increasing speed). D) Left: mean spike rates of Aδ-mechano-nociceptive fibers in the static phase in response to increasing force and (right) mean spike rates of D-hair fibers in the dynamic phase (in response to ramps of increasing speed) in WT and *Elkin1*$^{-/-}$ mice. Error bars indicate SEM.

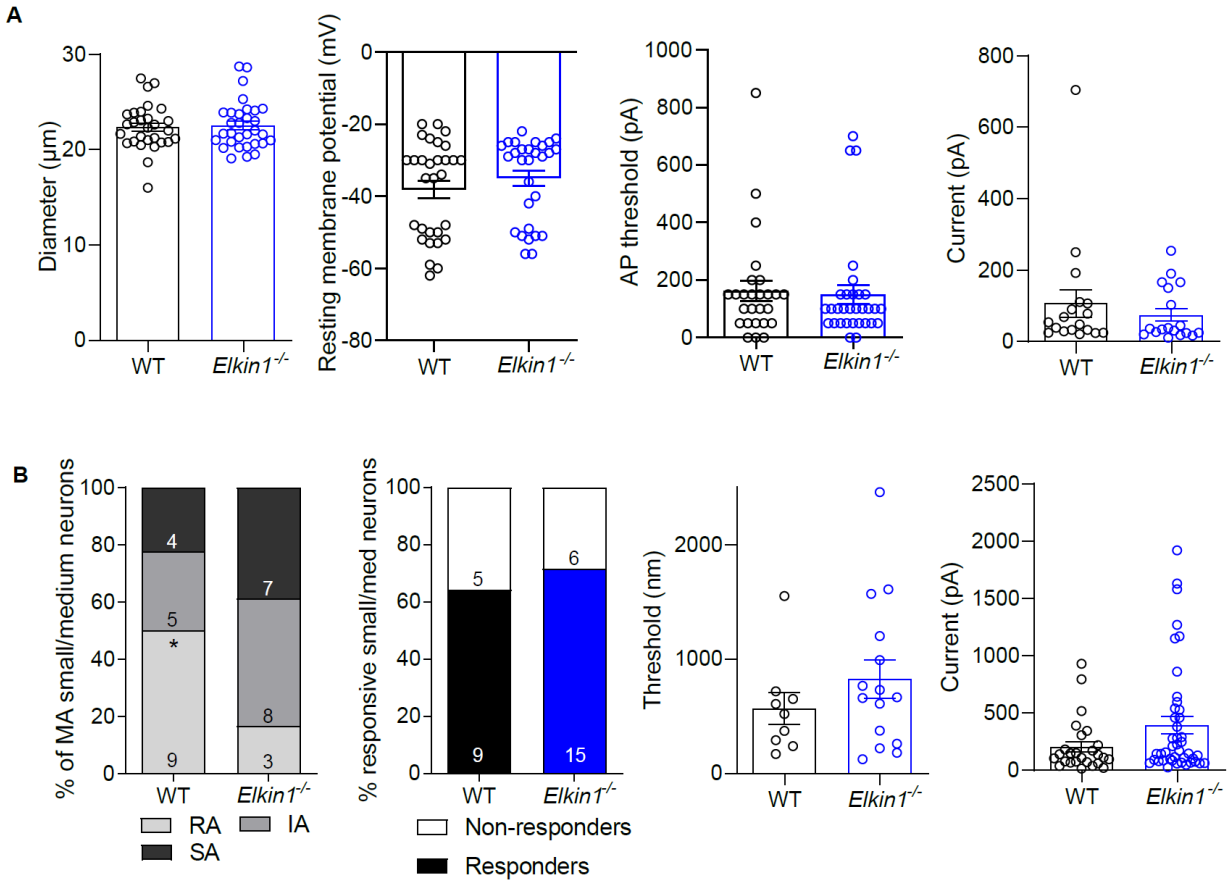

Fig S9: Electrophysiological properties of small/medium sensory neurons. A) Properties of neurons assessed using indentation assay including diameter, resting membrane potential, action potential firing threshold and amplitude of MA-currents. Each dot represents a neuron. B) Properties of small/medium neurons as assessed through pillar array assay including percent of MA neurons belonging to rapidly (RA), intermediately (IA) and slowly-adapting (SA) category, threshold of MA-current activation and max current amplitude of MA-currents. Each dot represents a neuron for threshold and each stimulus for current. Data obtained from both male and female mice. Proportions were compared using chi-sq tests. * indicates $p < 0.05$. Error bars indicate SEM

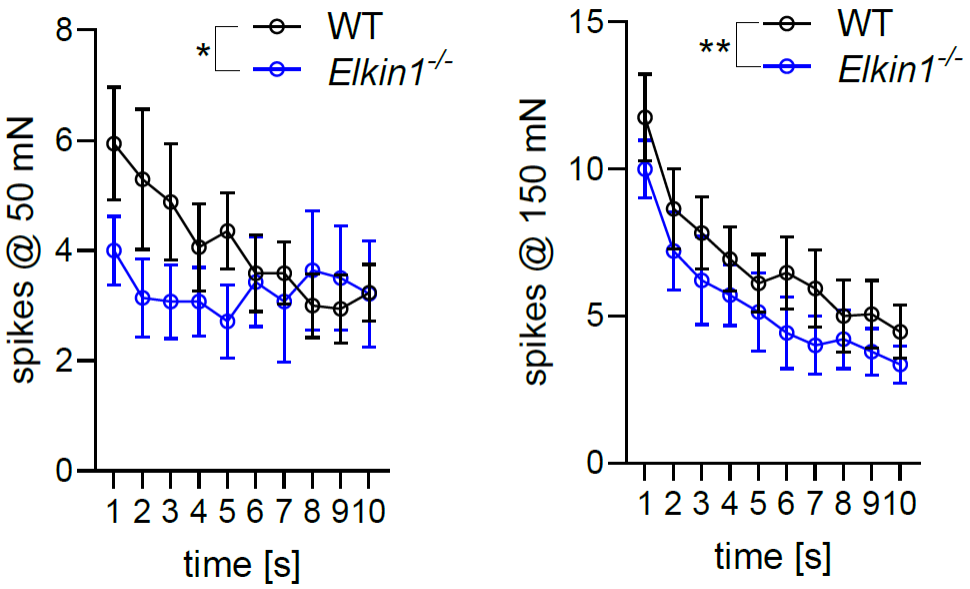

Fig S10: Electrophysiological properties of mechanosensitive C-fibers in the saphenous nerve. Graphs showing absolute number of spikes in response to 50 mN and 150 mN force applied for 10 s. Each dot represents average of n = 17 WT and n = 14 *Elkin1*$^{-/-}$ fibers. Data obtained from both male and female mice. Group comparisons were made using 2-way ANOVA followed by multiple comparison post hoc tests. * indicates $p < 0.05$, ** indicates $p < 0.01$. Error bars indicate SEM.

Table S1: Anatomical properties of the saphenous nerve assessed using electron microscopy.

Data table showing quantification of ultra-structure of saphenous nerve axons in WT and *Elkin1*$^{-/-}$ mice. Data obtained from 6 male mice, 15 images from each mouse were analyzed. Error bars indicate SEM.

	WT (n = 3)	***Elkin1*$^{-/-}$ (n = 3)**
Avg cross-sectional area of A-fibers	4.5 ± 0.2	4.4 ± 0.1
G ratio of A-fibers	0.69 ± 0.007	0.68 ± 0.008
Avg cross-sectional area of C-fibers	0.29 ± 0.05	0.29 ± 0.02
Total A-fibers (extrapolated)	565.0 ± 53.3	663.7 ± 104.9
Total C-fibers (extrapolated)	2935.0 ± 340.9	3108.0 ± 373.0
Ratio of A fibers to C fibers	5.3 ± 0.7	5.7 ± 1.1

Table S2: Frequency of births

Table showing absolute number and percentage of WT, *Elkin1*$^{+/-}$ and *Elkin1*$^{-/-}$ animals from a *Elkin1*$^{+/-}$ x *Elkin1*$^{+/-}$ breeding.

	WT	***Elkin1*$^{+/-}$**	***Elkin1*$^{-/-}$**
Number of animals	34	61	37
Percent of Total (n=132)	25.7	46.2	28